AD NUMBER
AD842013
LIMITATION CHANGES
TO: **Approved for public release; distribution is unlimited.**
FROM: **Distribution: Further dissemination only as directed by Air Force Space and Missile Systems Organization, Los Angeles, CA 90045, NOV 1967, or higher DoD authority.**
AUTHORITY
samso, usaf ltr, 28 feb 1972

(18) SAMSO (19) TR-68-44

(14) SRS-
Publication No. UG-4259

(1)

(9) TECHNICAL REPORT,

(6) TURBULENT FRONT STRUCTURE OF AN AXISYMMETRIC COMPRESSIBLE WAKE.

Monitored by: Space and Missile Systems Organization
Air Force Systems Command
Norton Air Force Base, California

Under Contract: (15) F04701-68-C-0032, ARPA Order-888

Sponsored by: Advanced Research Projects Agency
Department of Defense
ARPA Order No. 888

Prepared by: (10) Dr. A. Demetriades

(11) 15 Nov 67 (SMSD) 2 AFS Calif 90045

(12) 67p.

CORPORATION
-entry Systems
ch, California

BLANK PAGE

ABSTRACT

Intermittency measurements have been performed within the first one hundred virtual diameters of an axi-symmetric compressible wake. The primary measurements, performed with the hot-wire anemometer, concerned the intermittency factor and the frequency of zero occurrences. The intermittent flow covered most of the wake profile but for a narrow region about the axis, and was found to be normally distributed around the average front position. The latter, along with the extent of the front standard deviation, was found to agree numerically with expectations based on low speed wakes and to grow as the 1/3-power of axial distance. A weak periodicity of the front was detected at a wavelength about nine times greater than the longitudinal scale of turbulent velocity fluctuations. This periodicity affects the turbulent spectra.

FOREWORD

This report is the third in a series describing the properties of free compressible turbulent flows, including turbulent plasmas, stemming from a continuing research program on hypersonic wakes at Philco-Ford Corporation. The present work describes the intermittency characteristics of an axi-symmetric compressible wake whose mean and turbulence properties have been described in the two reports preceding it, "Mean Flow Measurements in an Axisymmetric Compressible Turbulent Wake" (No. U-3978, 1 March 1967) and "Turbulence Measurements in an Axi-Symmetric Compressible Wake" (No. UG-4118, 1 August 1967). The corresponding properties of a two-dimensional wake will be reported soon.

This research has been supported by the Advanced Research Projects Agency and monitored by the Space and Missile Systems Organization, USAF. The author acknowledges with gratitude the continuing encouragement of the Philco-Ford Corporation and the expert assistance of Mr. Lee Von Seggern with the measurements and the instrumentation.

NOMENCLATURE

A_n	coefficient of polynomial curve-fitting the intermittency factor
B_n	coefficient of polynomial curve-fitting the zero frequency
C_DA	(square of) virtual wake diameter
f	frequency; also, random function of Appendix B
f_T	frequency at front wavelength
H	jump across the front (Appendix B)
L	transverse scale of wake
L_o	wake half-radius
M	local Mach number
N	frequency of zero occurrences
N_o	value of N at $\bar{Y}$
N_{max}	maximum of N at each axial position
P	probability
R_T	turbulent Reynolds number
T	local temperature
$\tilde{T}$	non-dimensional temperature
u	local axial velocity
$\tilde{u}$	non-dimensional axial velocity
u_∞	free stream axial velocity
$u(\bar{Y})$	axial velocity at $\bar{Y}$
WEB-VI	computer program for data reduction (Appendix A)

X	Axial coordinate
$\bar{X}$	non-dimensional axial coordinate
X STATION	axial position at which data were taken
Y	radial coordinate
$\bar{Y}$	radial position of the front
Y'	radial position at which radial derivative of γ is zero
Y_{max}	radial position at which N is maximum
γ	intermittency factor; also, ratio of specific heats
Δ	r.m.s. fluctuation
η	non-dimensional radial coordinate
Λ_F	front autocorrelation microscale
Λ_F	average wavelength of front
Λ_u	longitudinal macroscale of velocity fluctuations
Λ_T	longitudinal macroscale of temperature fluctuations
ρ	local density
σ	standard deviation of front

CONTENTS

ILLUSTRATIONS

ILLUSTRATIONS (Continued)

ILLUSTRATIONS (Continued)

1. INTRODUCTION

It is well known that turbulent flows spreading into ambient, quiescent fluid are separated from the latter by a sharp, irregular front or interface. This front changes shape continuously with time, but on the average it advances into the ambient fluid engulfing the latter and making it turbulent. In shear turbulence this motion is accompanied by an overall movement of the front along the direction of the shearing motion as well. Thus, there are at least three practical objectives motivating the study of this front. First, its statistical properties are necessary for the quasi-steady geometrical description of shear zones such as boundary layers, jets and wakes. Secondly, the correct measurement of the net turbulence properties within the front requires the recognition and separation of those effects on the turbulence signal which are due to the intermittent nature of the front itself. Finally, the more detailed the understanding of ambient fluid engulfment and conversion is, the better will be the prediction of the bulk properties of the shear flow, such as thickness and lateral expansion. These objectives are particularly important for the hypersonic wake where the shape of the front envelope, its motion and its effect on the turbulence within it enter directly and quantitatively in computations of radar backscatter.

This report deals primarily with the geometrical features of the front and more specifically with the most probable front position, the standard deviation (a measure of the "wrinkle" amplitude), and the front microscale (a measure of the front wavelength). A considerable investigation

found can only be related to gross flight parameters (e.g., body shape and size) rather than the more meaningful integral wake properties (e.g., the drag, transverse scale, etc.) obtainable by a complete mapping of the flow field such as is possible in wind tunnels. The latter prerequisite has already been fulfilled in the present case, since complete flow maps of the axi-symmetric wake at hand were already available (References 9 and 10). Using this well-probed wake flow, two additional measurements were made: the intermittency factor was recorded with a special electronic circuit, and the frequency of "zero-occurrences" was also measured. Sufficient information was thus gathered to deduce (1) the position of the turbulent front, (2) the front standard deviation, and (3) the front microscale. Further use of these data can and will be made in deducing further turbulence properties of the wake.

2. WAKE MODEL AND FLOW FIELD

The wind tunnel, asixymmetric model and wake flow characteristics have already been described in References 9 and 10. The reader should consult these references for details and especially for that nomenclature not peculiar to the intermittency measurements themselves. A photographic and schematic view of the model appears on Figure 1.

3. PROCEDURE AND SPECIAL INSTRUMENTATION

The basic tool for intermittency measurements is a method capable of recording the time the hot-wire is immersed in the turbulent flow versus the time it is not. The simplest way to do this is to obtain a continuous direct record of the interface (e.g., hot-wire output versus time or a series of wake photographs) and to subject this record to statistical analysis; this method is in general awkward and inaccurate. A better way is to perform the statistics in situ by means of an electronic circuit such as used by Corrsin and Kistler (Reference 1) and Bradbury (Reference 11). The device described below is basically their design adapted to higher frequencies.

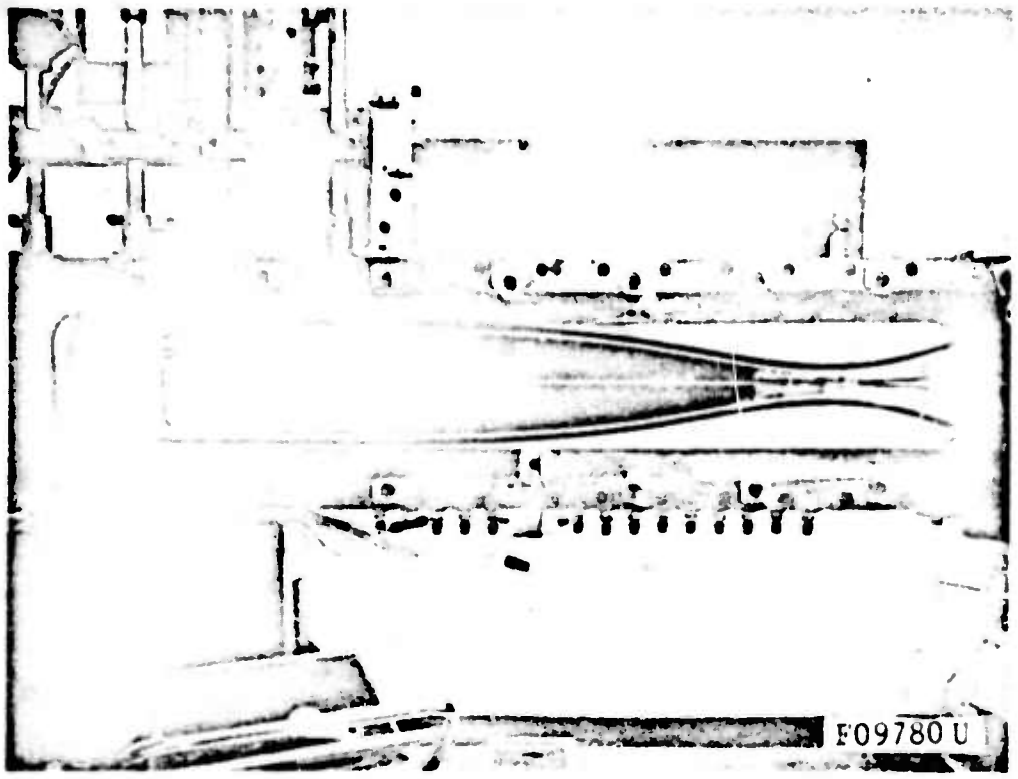

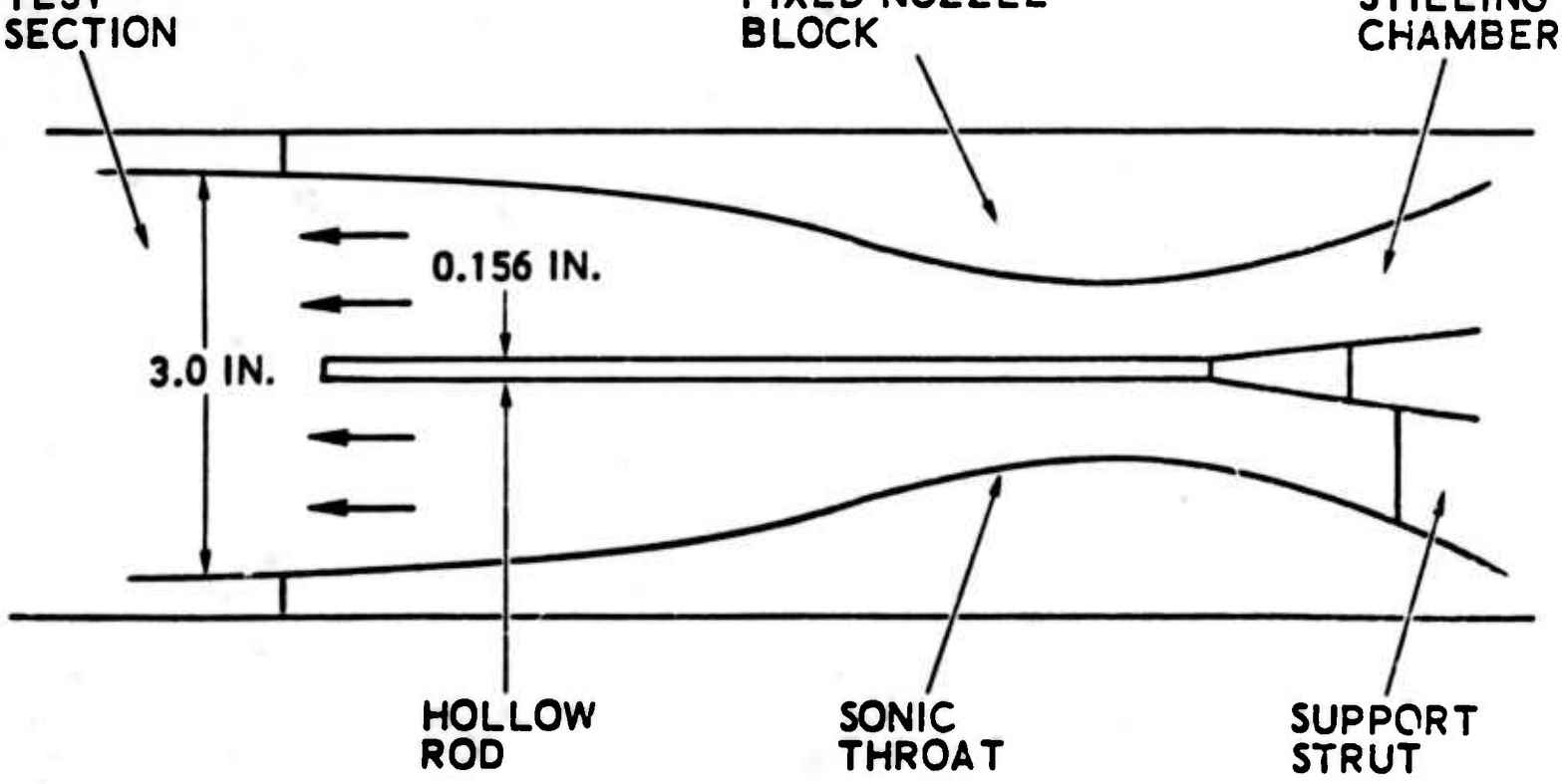

F09781 U

FIGURE 1. TOP: PHOTOGRAPH OF TEST SECTION SHOWING AXISYMMETRIC MODEL AT LEFT, PROBE AT LEFT AND PROBE ACTUATOR (TOP LEFT). BOTTOM: DETAILS OF THE AXISYMMETRIC MODEL.

of these features has been performed at low speeds with such flows as jets, wakes, and boundary layers: compendia of these studies have been presented by Corrsin and Kistler (Reference 1), and more recently by Townsend (Reference 2). These compendia show that the qualitative features of the front irregularity follow some general rules irrespective of flow geometry; on the other hand, quantitative differences, such as the ratio of the standard deviation σ to the average front position $\bar{Y}$, have been noted among boundary layers, jets, and wakes. Furthermore, corresponding front characteristics for the axisymmetric wake have not been reported to date in comparable thoroughness and detail, although some tentative intermittency observations in sphere wakes have been reported by Baldwin (Reference 3) and Gibson (Reference 4). A curious phenomenon recorded in the course of these studies is the appearance of rather extensive stretches of irrotational flow on the wake axis where fully turbulent flow is usually noted in the results of other experiments of this type (see Reference 1). Attempts to examine this phenomenon in the supersonic wake were made in the present experiment.

The main objective of this portion of the present work, however, was to study the effect of compressibility. High-speed measurements of the front structure are virtually nonexistent, with the exception of the statistical interpretation of ballistic-range photographs of wakes carried out to some detail by Schapker, Levensteins and Krumins, and Knystautas (References 5 through 7) respectively. This optical method has revealed certain important similarities between low- and high-speed front behavior as regards, for example, the distribution of intermittency factor and the front microscale.* Unfortunately the intermittent properties so

---

*There are several serious objections to the measurement of intermittency by the processing of photographs. For example, proper statistics of a stationary ensemble can be performed only if there are no gradients of the mean or root-mean-square values in the ensemble-i.e., if, for instance, the wake thickness is constant with distance; this is not so restrictive for small-scale turbulence studies[8] but for the interface, where the scales are large, it means that proper statistics can be performed from photographs only past some thousands of diameters. There are also the usual observational difficulties: prominences and ridges can be seen from the photographs, but "valleys" cannot.

An intermittency meter for measuring the intermittency factor of turbulent wakes directly from a hot-wire anemometer signal was fabricated for use in studying turbulent wake structure. The instrument utilizes seven Burr-Brown operational amplifiers and associated feed-back networks for signal conditioning. A signal level of up to 10 volts peak-to-peak can be handled effectively by this system making it compatible with the Transmetrics No. 6401-5 hot-wire anemometer amplifier. All Burr-Brown Amplifiers used in the system to condition the ac signal are 100 volts/ usec slewing rate providing an extremely fast response instrument for measuring the intermittency. This device, illustrated in Figures 2 and 3, also included a 0-to-1-volt dc output directly proportional to the intermittency factor, which could thus be read directly on the face of a panel meter or used to drive a dc recorder. It was initially hoped that the wire could be traversed continuously through the wake, and that the dc output noted directly on the recorder. As other investigators (Reference 1) also found, however, the trigger level and other circuit controls required adjustment from point to point, so that the intermittency measurement was not quite that simple. Nevertheless, the circuit performed satisfactorily despite the high frequency response required.

For these measurements, an oven-calibrated 0.00005-inch wire is used. This wire was processed as indicated in Reference 9 but was not flow-calibrated since the on-off process of intermittency requires no quantitative knowledge of the wire properties as such. The wire current was first adjusted as the maximum safe value so that no melting would occur anywhere across the wake and its time constant adjusted to the proper value; it was then lowered at a point in the wake and, after suitable adjustment of the circuit controls, the intermittency factor (or the frequency of zeros) was noted. The block diagram employed is shown in Figure 4.

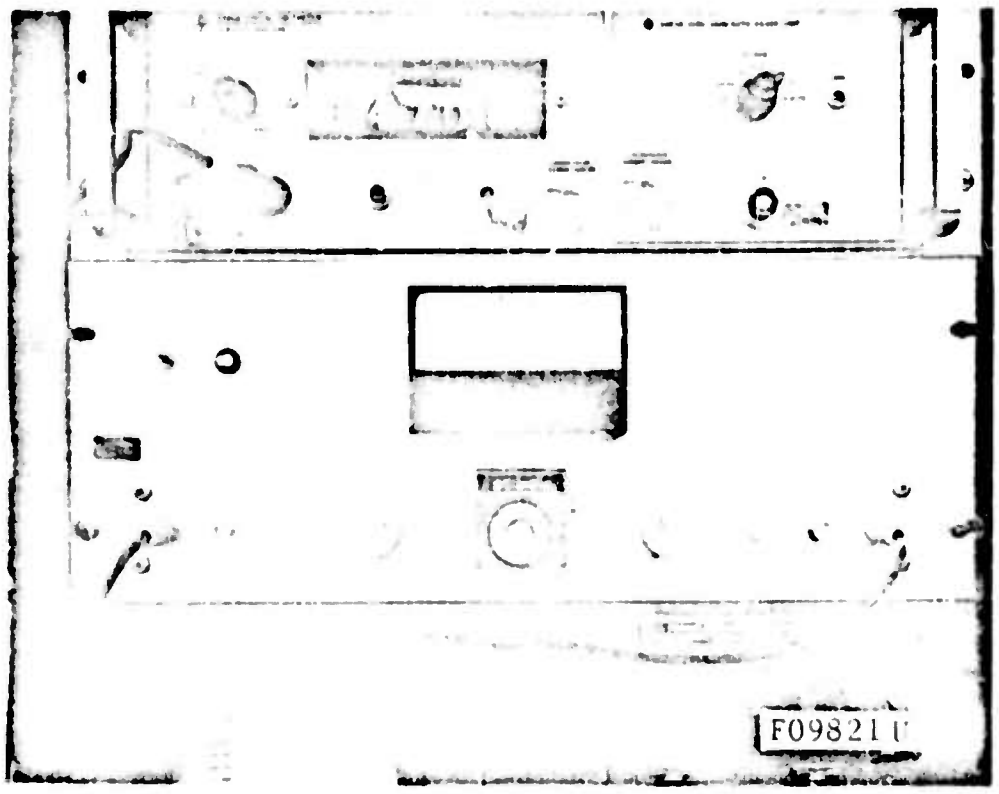

FIGURE 2. PHOTOGRAPH OF INTERMITTENCY CIRCUIT (CENTER)

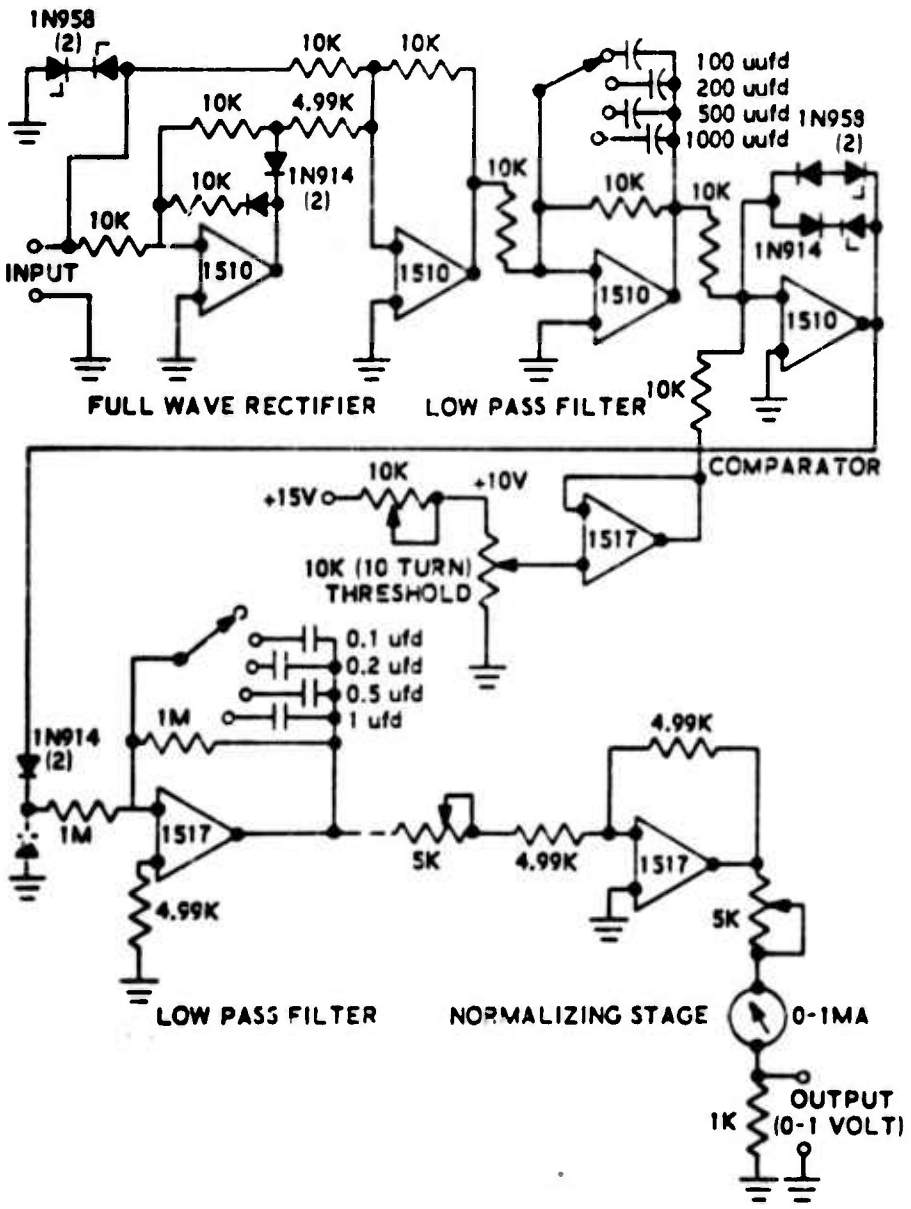

FIGURE 3. ELECTRONIC CIRCUIT OF THE INTERMITTENCY FACTOR

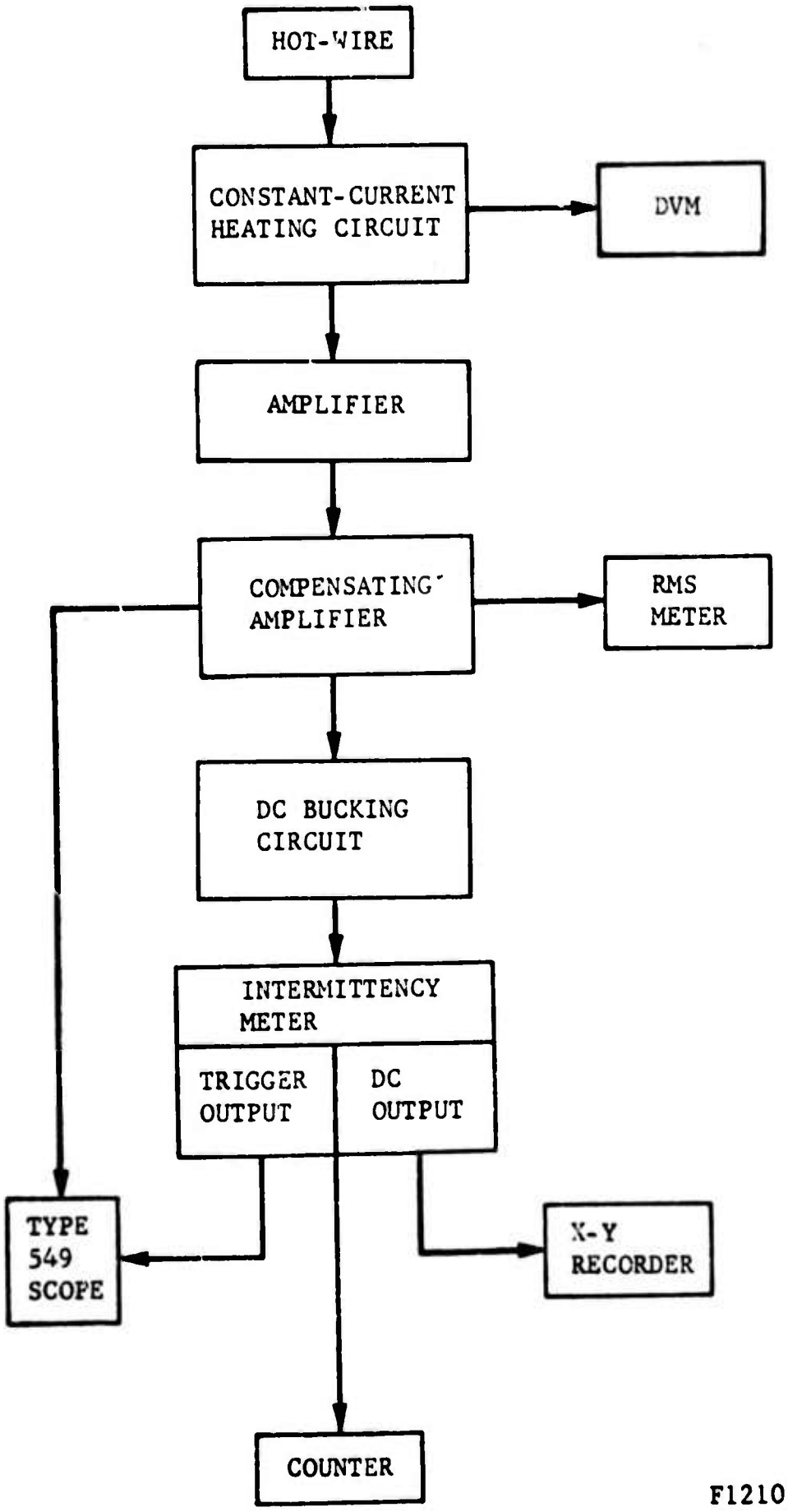

F12101 U

FIGURE 4. DIAGRAM OF ELECTRONICS USED FOR INTERMITTENCY MEASUREMENT

3.1 PROCEDURE FOR INTERMITTENCY MEASUREMENT

The intermittency factor $0 < \gamma < 1$ was measured at each of about 22 radial position and at each of the 14 axial positions (XSTATIONS 0 through 13) at which all measurements with the axisymmetric wake were made. At each point the signal was first observed on the Tektronix type 549 storage oscilloscope for the purpose of making the required adjustments in signal amplification and especially in the trigger level. The trace storage technique, a new development in oscillography, proved an invaluable aid in recording γ correctly. By freezing the trace on the scope screen for an arbitrary controllable period (from a fraction of a second to one hour) the operator can determine much better than hitherto possible whether the Schmidt circuit triggers properly. Typical dual traces thus obtained are shown in Figure 5. In these, the up position of the trigger output trace marks the time the wire is within the turbulent fluid; the ratio of this time to the down time is given by the circuit directly as the fraction of one volt dc (e.g., 0.68 volt denotes $\gamma = 0.68$).

3.2 PROCEDURE FOR MEASURING THE ZERO OCCURRENCES

The rectangular-pulse shape of the trigger output shown on Figure 5 affords a relatively simple way by which the frequency of the wire crossings across the wake front can be measured. This was done by directing the trigger output signal into a counter whose own trigger level was set below 1 volt dc. The crossing frequency (also called the frequency of zero occurrences or zeros) was then read directly by the counter. This measurement was also made at each of the 14 XSTATIONS, although at fewer radial positions for each. Reading the zero frequencies required, of course, the same adjustments of the intermittency circuit and amplifier as during the measurement of γ.

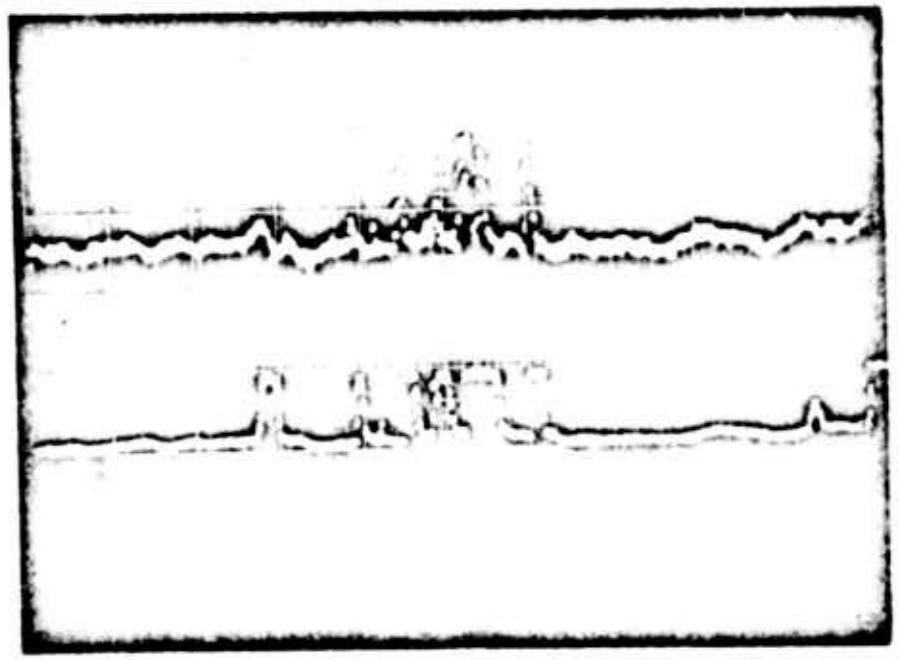

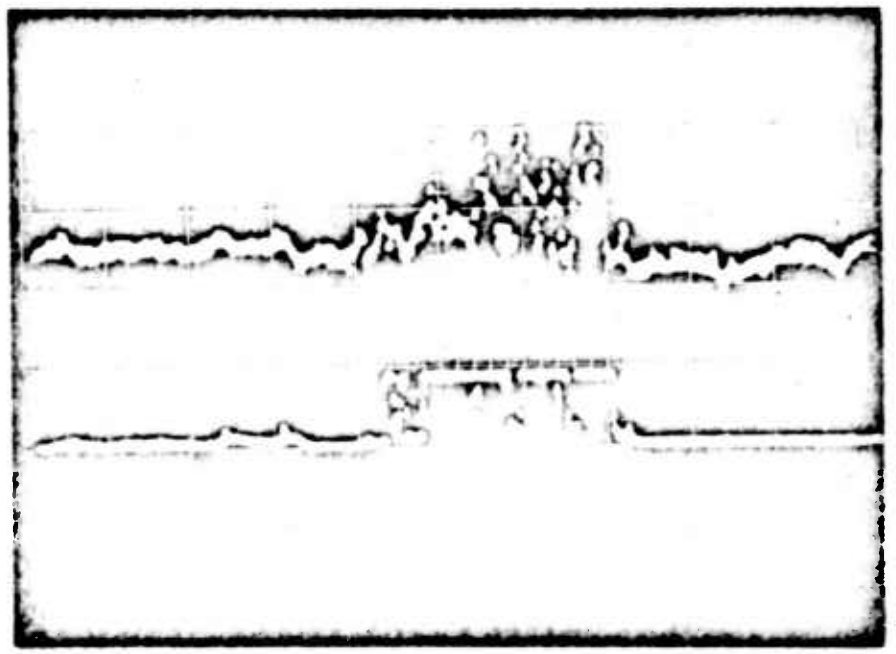

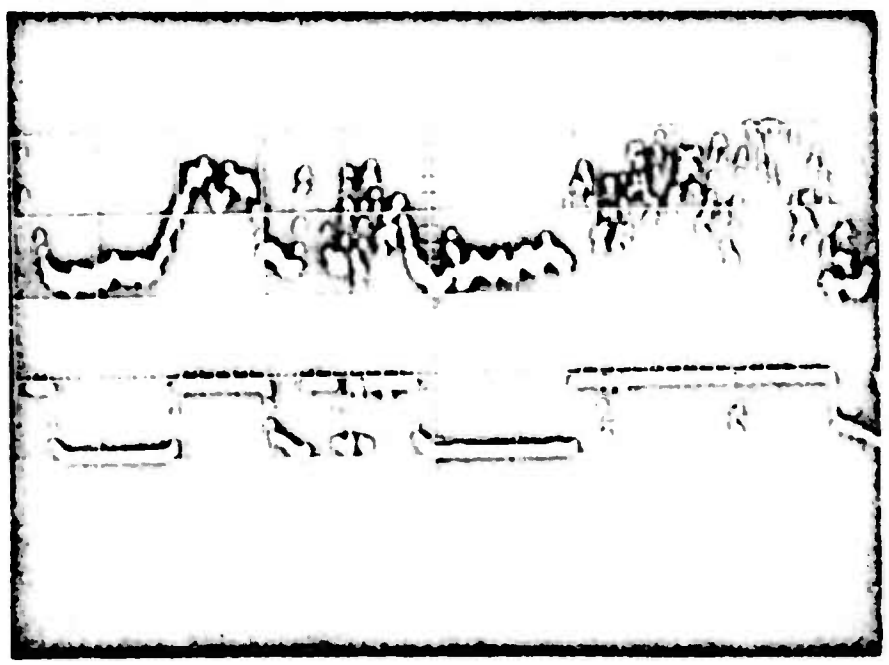

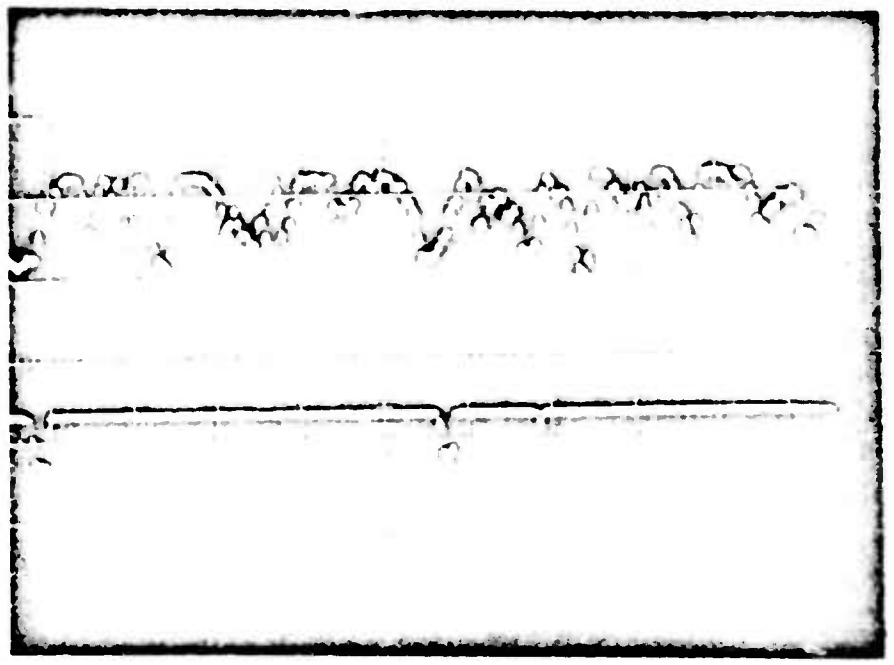

FIGURE 5. TYPICAL OSCILLOGRAMS OF INTERMITTENT BEHAVIOR: TOP TRACE OF EACH IS HOT-WIRE OUTPUT, BOTTOM TRACE IS TRIGGER OUTPUT. INTERMITTENCY FACTORS ARE: TOP LEFT, 0.05; TOP RIGHT, 0.17; BOTTOM LEFT, 0.43; BOTTOM RIGHT, 0.99

F12102

4. DEFINITIONS OF FRONT PROPERTIES

A thorough discussion of the processing and interpretation of intermittency measurements, together with the necessary background from the theory of stationary random variables, has been given by Corrsin and Kistler (Reference 1). The formulas necessary to process the data as obtained above will be given below.

Because the probability P of the existence of the turbulent front is

$$P = d\gamma/dY \tag{1}$$

where Y is the radial coordinate, it follows that the most probable position $\overline{Y}$ of the front is

$$\overline{Y} = \int_0^\infty Y \frac{d\gamma}{dY}\, dY \tag{2}$$

The quantity $\overline{Y}$ is very crucial to the geometric description of a turbulent wake and is, in fact, the only rational definition of the surface bounding the turbulent fluid in the average or steady-state sense.

Another important definition is the mean standard deviation of the front corrugations

$$\sigma \equiv \left[\int_0^\infty (Y-\overline{Y})^2 \frac{d\gamma}{dY}\, d\,(Y-\overline{Y})\right]^{\frac{1}{2}} \tag{3}$$

where the lower limit of zero is proper only if $d\gamma/dY$ and $d^2\gamma/dY^2$ are also zero at $Y = 0$. In addition to $\overline{Y}$ and σ, a third quantity of geometrical importance is the autocorrelation microscale of the front

$$\overline{\lambda}_F = \frac{\sqrt{2}}{\pi} \frac{\overline{U}}{N_o} \frac{\overline{Y}}{} \tag{4}$$

where $U_{\bar{Y}}$ is the mean flow velocity at the front location (that is, $U_{\bar{Y}} \equiv U(\bar{Y})$) and where N_o is the average number of zeros at $Y = \bar{Y}$. Again the latter definition is appropriate to a normal (Gaussian) distribution of γ and its moments.

5. RESULTS

5.1 INTERMITTENCY MEASUREMENT

Figure 6 shows the distribution with radius of the intermittency factor γ at each of the 14 axial positions examined. Nearer the body the region of fully turbulent fluid ($\gamma = 1$) is noticeably broader around the axis, but further downstream γ departs from unity almost immediately off the axis. It appears, therefore, that in the self-preserving region (established in Reference 9 to lie beyond $\bar{x} = 40$) the fully turbulent fluid is confined to the very immediate vicinity of the wake axis; this is in general agreement with the two-dimensional wake at low speeds (Reference 12). The reader should not misinterpret, of course, the fully turbulent region as enclosed by a smooth surface of vanishingly small radius; statistically, this region can at times be of diameter comparable to the wake diameter. All Figure 6 implies is that the occurrence, if any, of laminar spots on the axis is highly improbable, in noteworthy contrast to the extent to which such spots appeared in the sphere wakes of Gibson (Reference 3) and Baldwin (Reference 4). In fact, a separate experiment was performed wherein 154 oscillograms of the turbulence on the axis were obtained, of which not one showed evidence of laminar (external) flow. Each of these was of 200 microseconds duration which, at a wake thickness of order 1 centimeter and a stream speed of about 60,000 centimeters per second, confirms conclusively the high improbability of $\gamma < 1$ on the axis.

Figure 7 shows (in more detail than Figure 6) a comparison (at a typical $\bar{x}$) of the distribution in γ and in the velocity $\tilde{u}$ and temperature $\tilde{T}$, the latter two as obtained in Reference 9. It is significant that turbulent

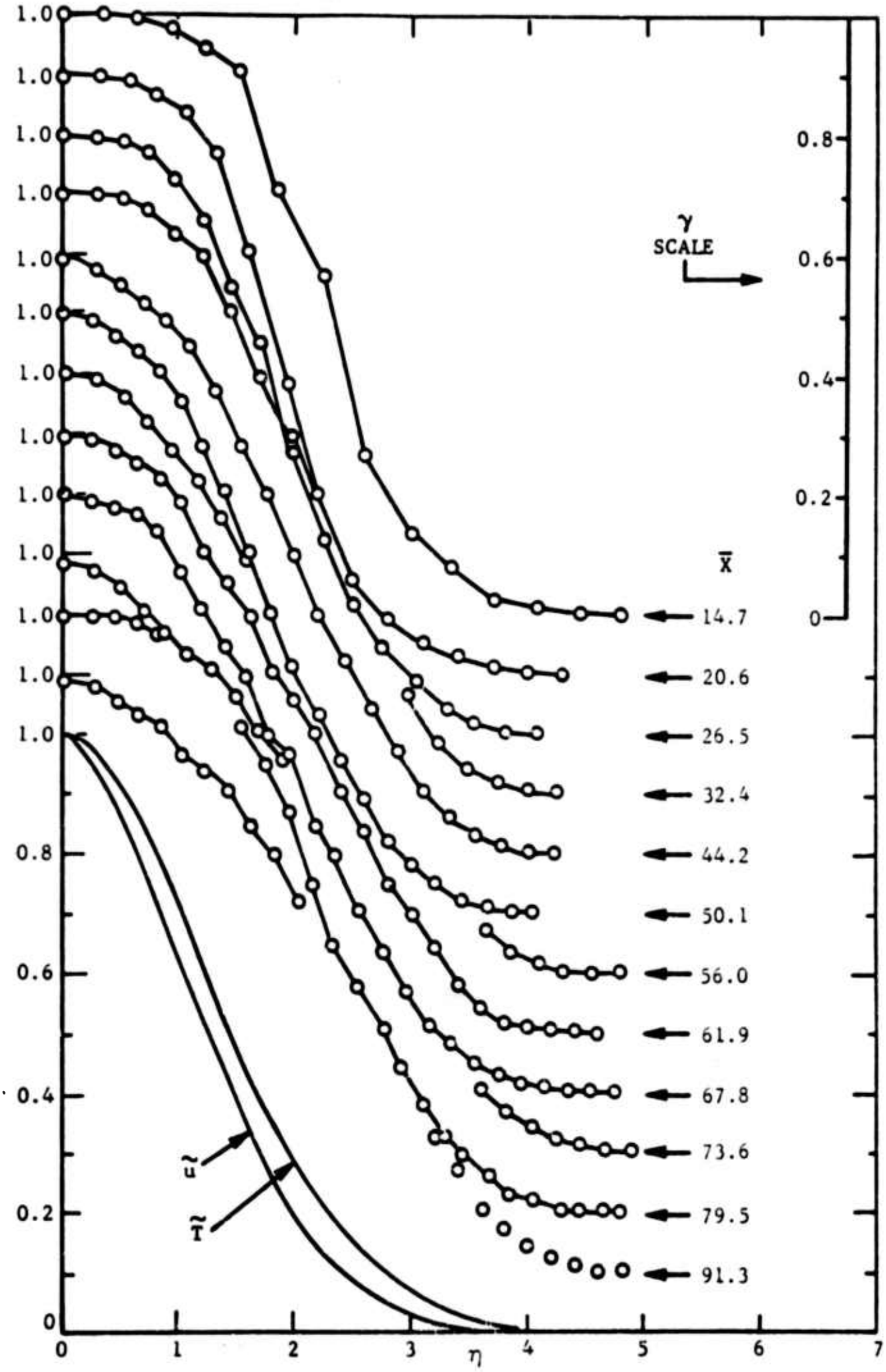

F12103 U

FIGURE 6. RADIAL DISTRIBUTION OF INTERMITTENCY FACTOR, WITH VELOCITY AND TEMPERATURE PROFILES SHOWN FOR COMPARISON

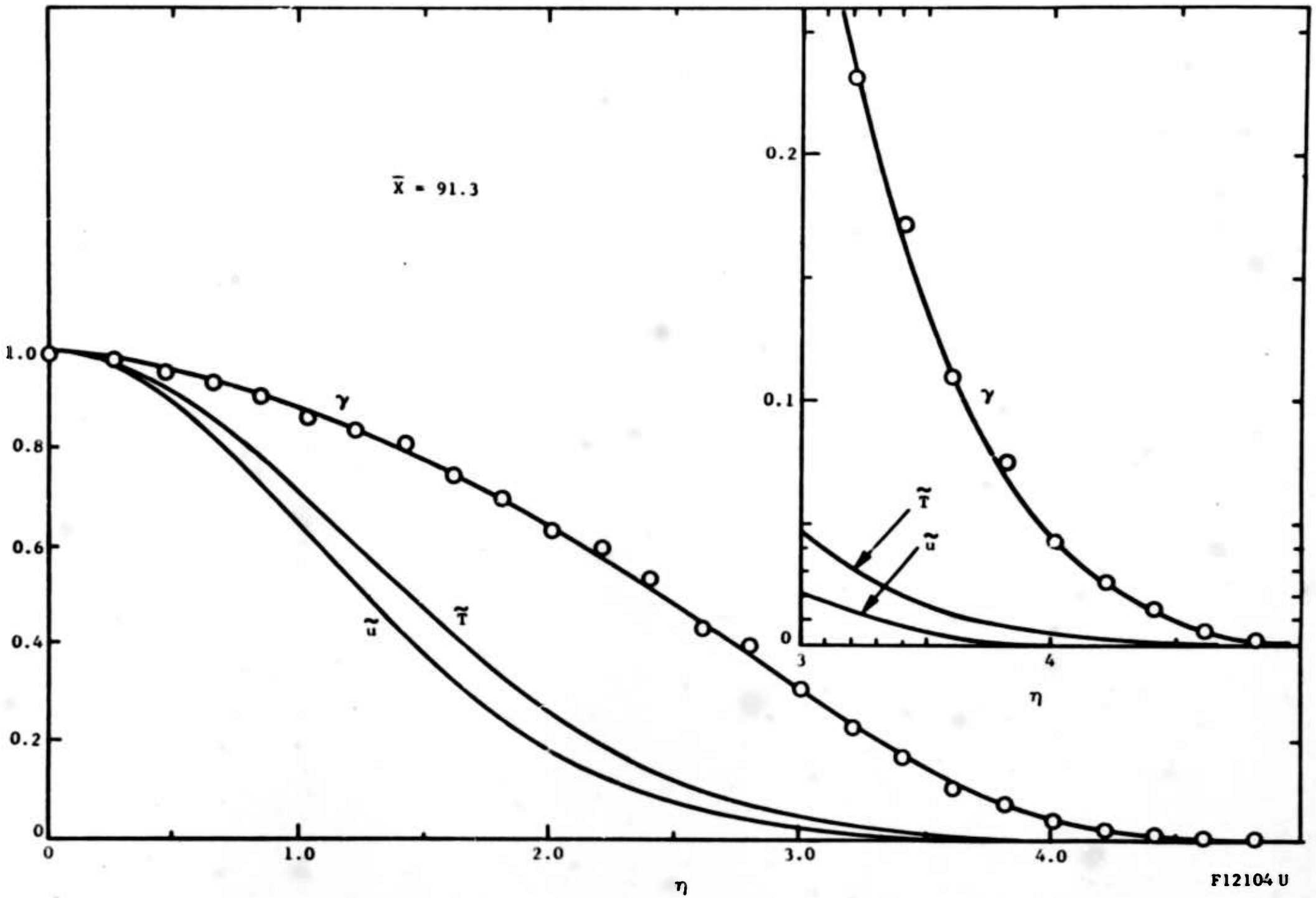

FIGURE 7. DETAILED COMPARISON OF TYPICAL INTERMITTENCY, VELOCITY, AND TEMPERATURE PROFILES

bursts appear at the edges of the wake (especially at high $\bar{x}$) where the sensible axial wake motion has all but vanished. In Figure 7 for example and at $\eta = 3.28$, $\tilde{u} = 0.01$ while $\gamma = 0.17$. We shall later discuss this phenomenon further.

In order to proceed with the computation of $\bar{Y}$ and σ which involves moments of γ, the distributions of Figure 6 were curve-fitted by polynomials of the form

$$\gamma = \sum_n A_n Y^n \qquad (5)$$

with the aid of program WEB-VI written for the Philco 2000 digital computer (see Appendix A). Adequate fits were obtained for 6th to 8th order polynomials, depending on the XSTATION, the aim being to minimize the computed standard deviation between the polynomial and the experimental curve. Table I shows the coefficients A_n for each XSTATION. By means of these polynomials and the aid of Equations (2) and (3) the following quantities were computed:

The quantity $\bar{Y}$ was computed as shown in Equation (2) and is pictured on Figures 8 and 9. The former shows that the variation $\bar{Y} = \bar{Y}(\bar{x})$ follows closely an 1/3-power dependence, which is natural to expect because the wake itself grows as $\bar{x}^{-1/3}$. The $\bar{Y}$ should therefore scale as L, the transverse wake scale which grows as $\bar{x}^{-1/3}$ also (Reference 9) and this is shown on Figure 9. The average of the points lies at $\bar{Y}/L = 2.11$, that is about two-thirds* of the wake "radius" out from the axis in terms of the non-dimensional radius $\eta \equiv Y/L$. Figure 10 shows that $\bar{Y}$ lies very close to the maximum Y' of the probability distribution $d\gamma/dY$ implying that the skewness of this distribution is negligible. The mean standard deviation σ of the front corrugations was computed from Equation (3). Figure 8 shows that in

---

*Rather than three-fourths as Townsend remarked qualitatively (Reference 2, p. 693).

TABLE I

COEFFICIENTS OF CURVE-FITTING POLYNOMIALS FOR INTERMITTENCY FACTOR

XSTA	$\bar{x}$	A_1	A_2	A_3	A_4	A_5	A_6	A_7	A_8
0	14.7	1.004	-1.015	-46.03	4,489	-97,470	7.827×10^5	-2.705×10^6	3.423×10^6
1	20.6	1.002	0.6643	-162.4	7,356	-1.349×10^5	1.051×10^6	-3.674×10^6	4.786×10^6
2	26.5	0.9993	1.296	-138.5	4,193	-64,250	4.426×10^5	-1.393×10^6	1.648×10^6
3	32.4	0.9995	0.0827	4.340	-398.6	800.4	5,497	-14,540	0
4	38.3	0.9993	-0.4189	21.98	-1,360	15,730	-90,588	2.639×10^5	-3.022×10^5
5	44.2	0.9967	-2.518	65.58	-1,200	6,932	-16,890	15,320	0
6	50.1	1.002	-1.672	45.79	-1,033	6,414	-17,040	19,210	-5,835
7	56.0	1.001	-0.0249	-53.09	497.3	-3,061	9,289	-10,170	0
8	61.8	0.9978	-0.1471	-2.259	-471.6	4,871	-22,830	52,440	-46,670
9	67.8	0.9964	0.6020	-34.23	122.2	-571.5	2,147	-2,687	0
10	73.6	0.9859	0.1840	-92.72	1,634	-13,840	56,670	-1.102×10^5	82,280
11	79.5	1.005	-1.504	48.06	-561.0	1,023	5,508	-22,130	21,900
12	85.4	1.003	-1.635	36.56	-522.9	2,209	-3,770	2,267	0
13	91.3	0.9884	-0.0427	-37.77	404.1	-2,511	6,890	-6,622	0

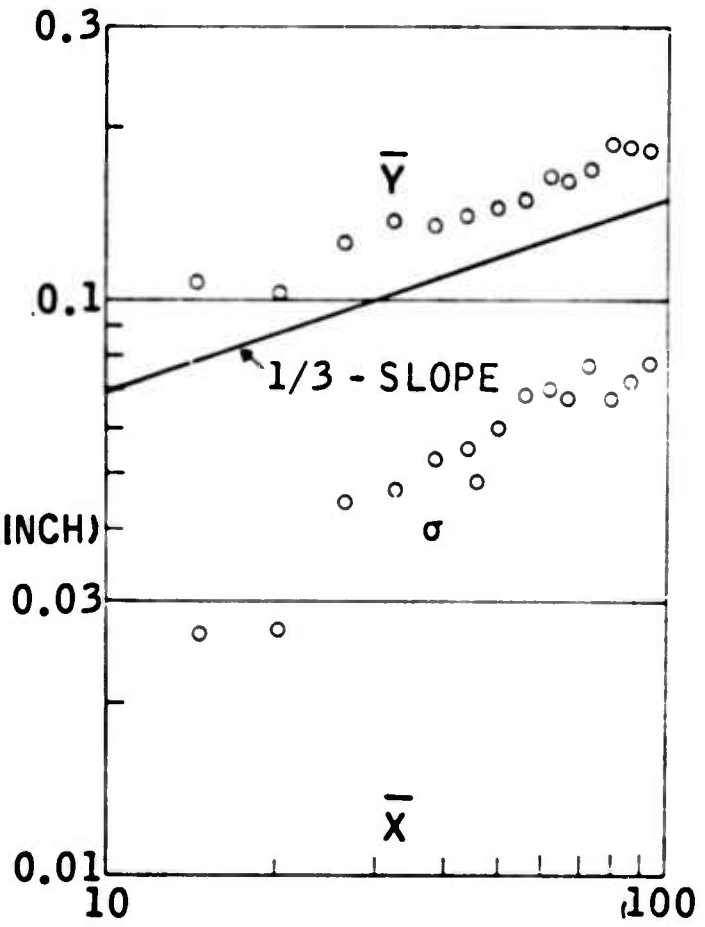

F12105 U

FIGURE 8. AXIAL VARIATION OF FRONT LOCATION AND STANDARD DEVIATION

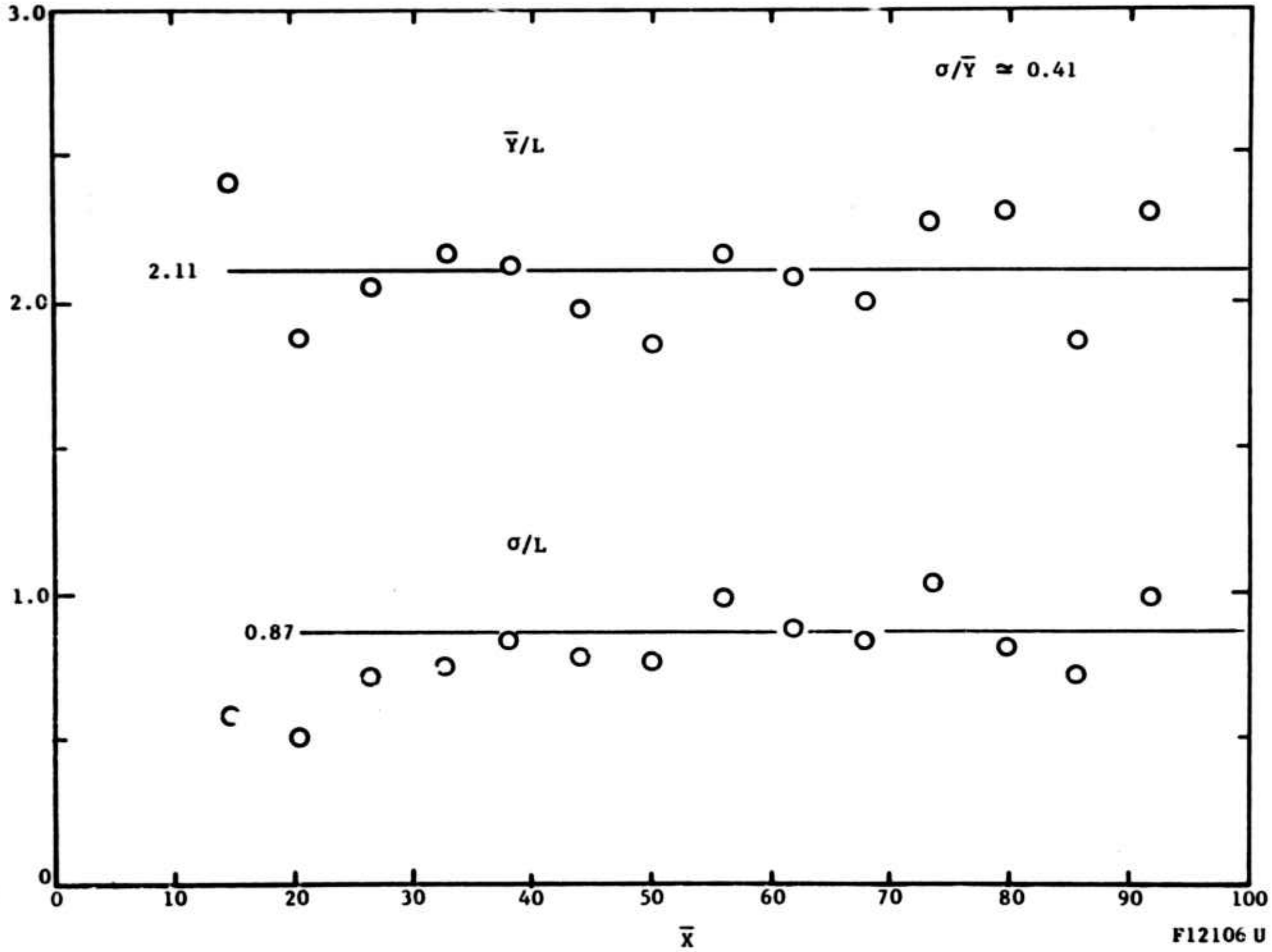

FIGURE 9. RELATIVE MAGNITUDES OF THE FRONT LOCATION, STANDARD DEVIATION, AND TRANSVERSE SCALE

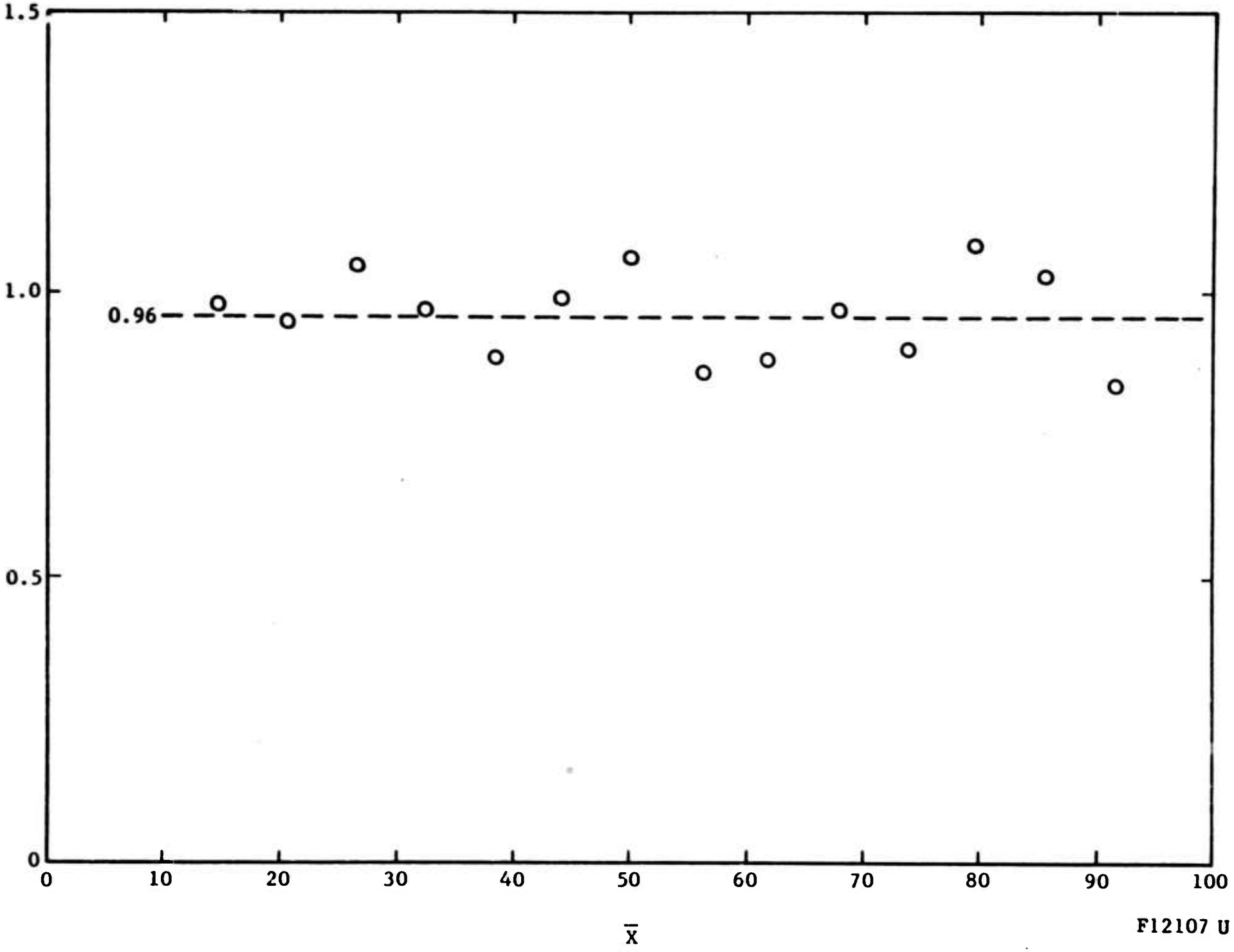

FIGURE 10. RELATIVE MAGNITUDES OF THE FRONT LOCATION AND THE MAXIMUM OF THE GAUSSIAN DERIVATIVE

dimensional form the standard deviation also follows the 1/3 increase with distance past about $\bar{x} = 40$, and the appropriate scaling with L is shown in Figure 9; the σ is, on the average, 0.87L.

Using the computed value of σ it is possible to plot the distribution of the factor γ about the front position $\bar{Y}$, as shown on Figure 11. With the exception of the initial two XSTATIONS, all data points fall on a well defined curve which is in fact identical to that encountered for most other free turbulent flows (Reference 1). The distribution of intermittency across turbulent interface appears to universally obey the Gaussian distribution shown in the latter illustration. The agreement between the present experiment and those of other authors will be shown in a later illustration.

5.2 MEASUREMENT OF ZEROS; FRONT MICROSCALE

Figure 4 shows the circuit used to read the frequency of zeros. As expected, very few events are noted at the extremities of the wake or near the axis. The frequency is thus zero on the axis and outside the wake and it is expected to peak near the turbulent front. The data are shown on Figure 12 for all XSTATIONS examined. The distribution of the zeros N about the mean is quite symmetric and the shift of the Y_{max} (N_{max}) with $\bar{x}$ is quite clear. The peak frequency, originally lying at about 20 kcps gradually shifts to about 30 kcps far downstream. The N_{max} and Y_{max} were found by again curve-fitting the data of Figure 12 with polynomials of the type

$$N = \sum_n B_n Y^n \qquad (6)$$

whose coefficients are given in Table II. The proper polynomial at each XSTATION was again found by minimizing its standard deviation from the experimental curve.

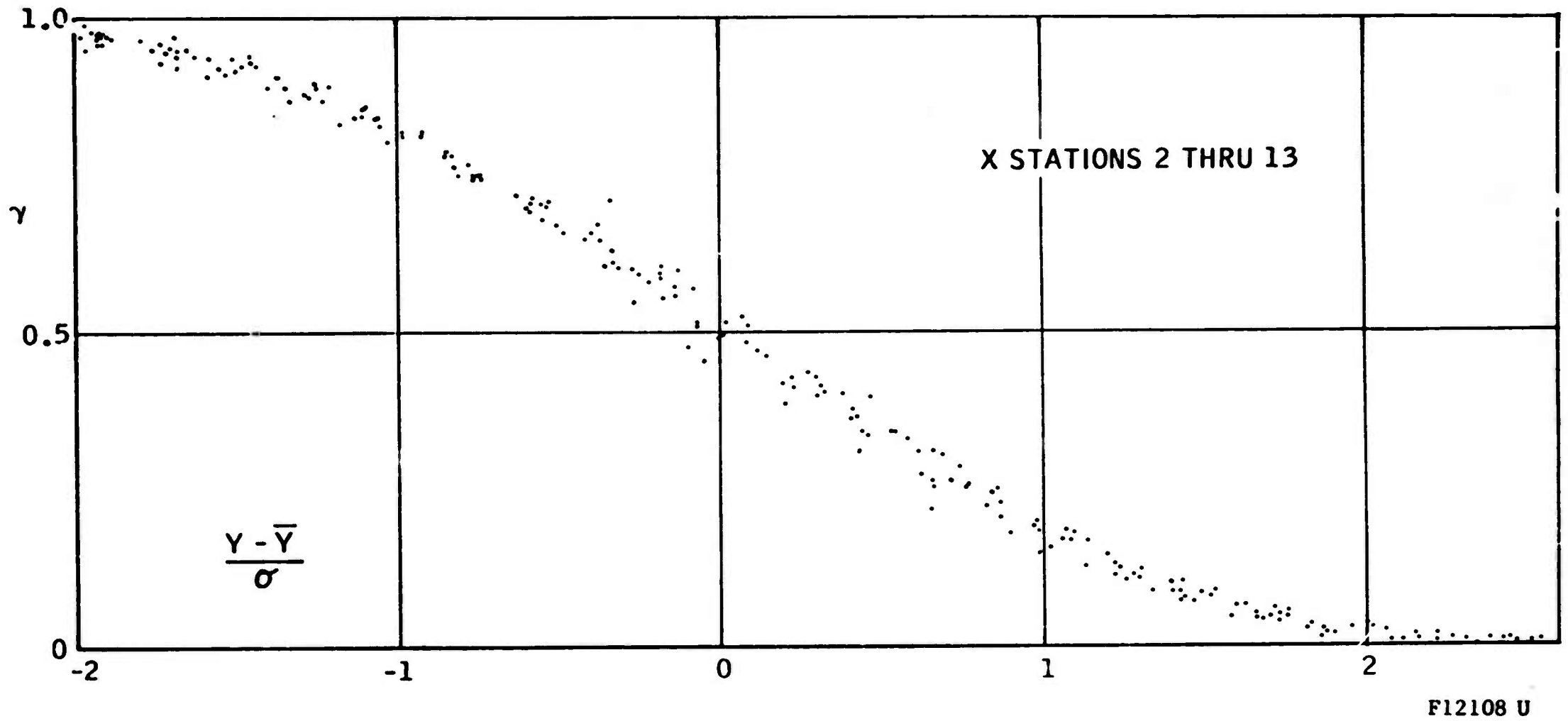

FIGURE 11. DISTRIBUTION OF INTERMITTENCY FACTOR ABOUT FRONT LOCATION

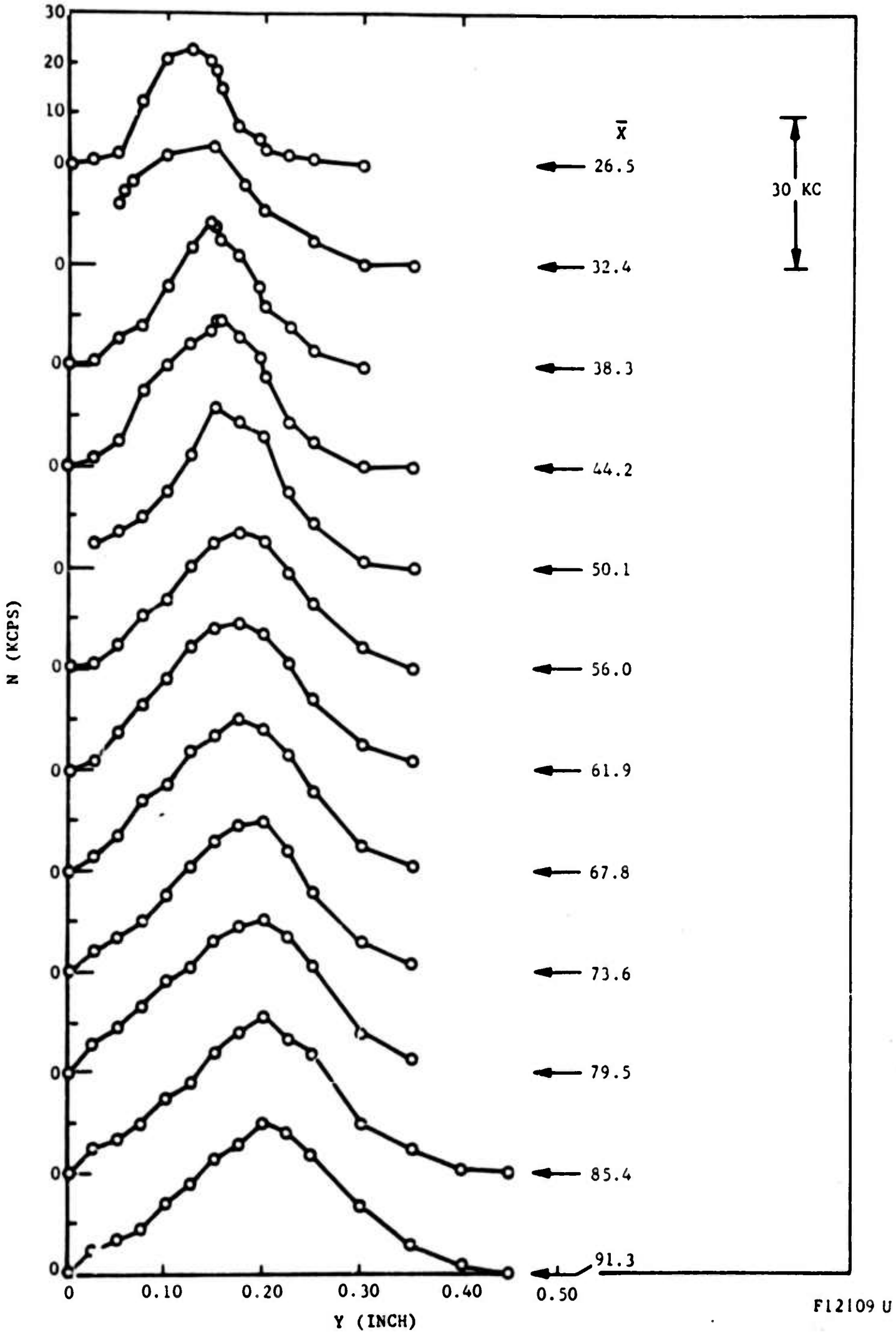

FIGURE 12. RADIAL DISTRIBUTION OF ZERO FREQUENCY

TABLE II

COEFFICIENTS FOR CURVE-FITTING POLYNOMIALS FOR ZERO OCCURRENCES

XSTA	$\bar{x}$	B_1	B_2	B_3	B_4	B_5	B_6	B_7	B_8
0	14.7	-108	1.47×10^{6}	-1.05×10^{8}	2.67×10^{9}	-3.08×10^{10}	1.79×10^{11}	-5.14×10^{11}	5.81×10^{11}
1	20.6	23.4	1.04×10^{6}	-7.52×10^{7}	1.99×10^{9}	-2.30×10^{10}	1.30×10^{11}	-3.61×10^{11}	3.92×10^{11}
2	26.5	204	4.41×10^{5}	-3.37×10^{7}	8.71×10^{8}	-9.2×10^{9}	4.66×10^{10}	-1.13×10^{11}	1.07×10^{11}
3	32.4	-52	5.80×10^{5}	-1.79×10^{7}	3.50×10^{8}	-3.21×10^{9}	1.43×10^{10}	-3.08×10^{10}	2.55×10^{10}
4	38.3	74	1.88×10^{5}	-7.64×10^{6}	1.36×10^{8}	-5.40×10^{8}	-2.09×10^{9}	1.65×10^{10}	-2.57×10^{10}
5	44.2	250	1.67×10^{4}	5.28×10^{5}	5.40×10^{7}	-5.79×10^{8}	1.96×10^{9}	-2.17×10^{9}	0
6	50.1	-212	5.40×10^{5}	-1.84×10^{7}	2.73×10^{8}	-1.69×10^{9}	4.51×10^{9}	-4.38×10^{9}	0
7	56.0	165	-9.94×10^{4}	8.09×10^{6}	-1.31×10^{8}	1.24×10^{9}	-6.33×10^{9}	1.56×10^{10}	-1.45×10^{10}
8	61.8	74.9	7.86×10^{4}	3.76×10^{5}	2.58×10^{7}	-2.55×10^{8}	7.62×10^{8}	-7.38×10^{8}	0
9	67.8	-126	2.01×10^{5}	-3.03×10^{6}	5.82×10^{7}	-3.89×10^{8}	1.02×10^{9}	-9.16×10^{8}	0
10	73.6	-109	3.22×10^{5}	-8.08×10^{6}	1.16×10^{8}	-6.66×10^{8}	1.62×10^{9}	-1.41×10^{9}	0
11	79.5	47.9	2.88×10^{5}	-2.92×10^{6}	1.68×10^{7}	8.89×10^{7}	-1.15×10^{9}	3.48×10^{9}	-3.33×10^{9}
12	85.4	-273	4.48×10^{5}	-1.18×10^{7}	1.56×10^{8}	-9.21×10^{8}	-2.64×10^{9}	-3.63×10^{9}	1.94×10^{9}
13	91.3	-81.3	3.73×10^{5}	-9.01×10^{6}	1.16×10^{8}	-6.63×10^{8}	1.81×10^{9}	-2.36×10^{9}	1.17×10^{9}

Several features of these data demand further examination. It is natural to suppose that the gradual spread of the curves of Figure 12 with $\bar{x}$ represent the physically enlarging intermittent zone (i.e., the standard deviation σ) and that the shift of the position of N_{max} corresponds to the increasing $\bar{Y}$ along the wake, as shown on Figure 8. In studying the latter point, the ratio $\bar{Y}/Y_{max}$ was plotted as shown on Figure 13 and was found to agree with unity to within 4 percent. Furthermore, the frequency N_o of zero occurrences at $\bar{Y}$ (obtained by computing N_o from Figure 12 at the position $\bar{Y}$) is identical with N_{max}, as shown in Figure 14. The turbulent front position corresponds, therefore, with the radial distance from the axis where the frequency of zero occurrences is a maximum. Finally, the symmetry of these occurrences was checked by plotting the normalized zero frequency N/N_{max} about Y/Y_{max}. The symmetry of these results, shown inFigure 15, is gratifying and the resemblance to a Gaussian distribution is quite close.

It should be mentioned that the measurement of the zeros in the manner described is neither versatile nor unambiguous. Much depends on that portion of the "intermittency circuit" which rectifies the hot-wire output. If the rectifying ("mean-squaring") process is too slow then the high-frequency events in the wake (in this case extending to some hundreds of kilocycles) cannot be detected. Of the process is too fast the Schmidt trigger fires many times while the wire is within the turbulence, not just when it enters or leaves it; an artificial increase of N is thus observed. By contrast the latter problem would not affect greatly the measurement of intermittency factor, where only the total time of immersion in turbulence is of importance. As before, the storage oscilloscope was of great assistance in resolving this question.

Because both the intermittency factor γ and the zeros N are distributed in a normal (Gaussian) fashion as shown by the preceding figures, it is possible to evaluate the autocorrelation microscale of the turbulent front in the

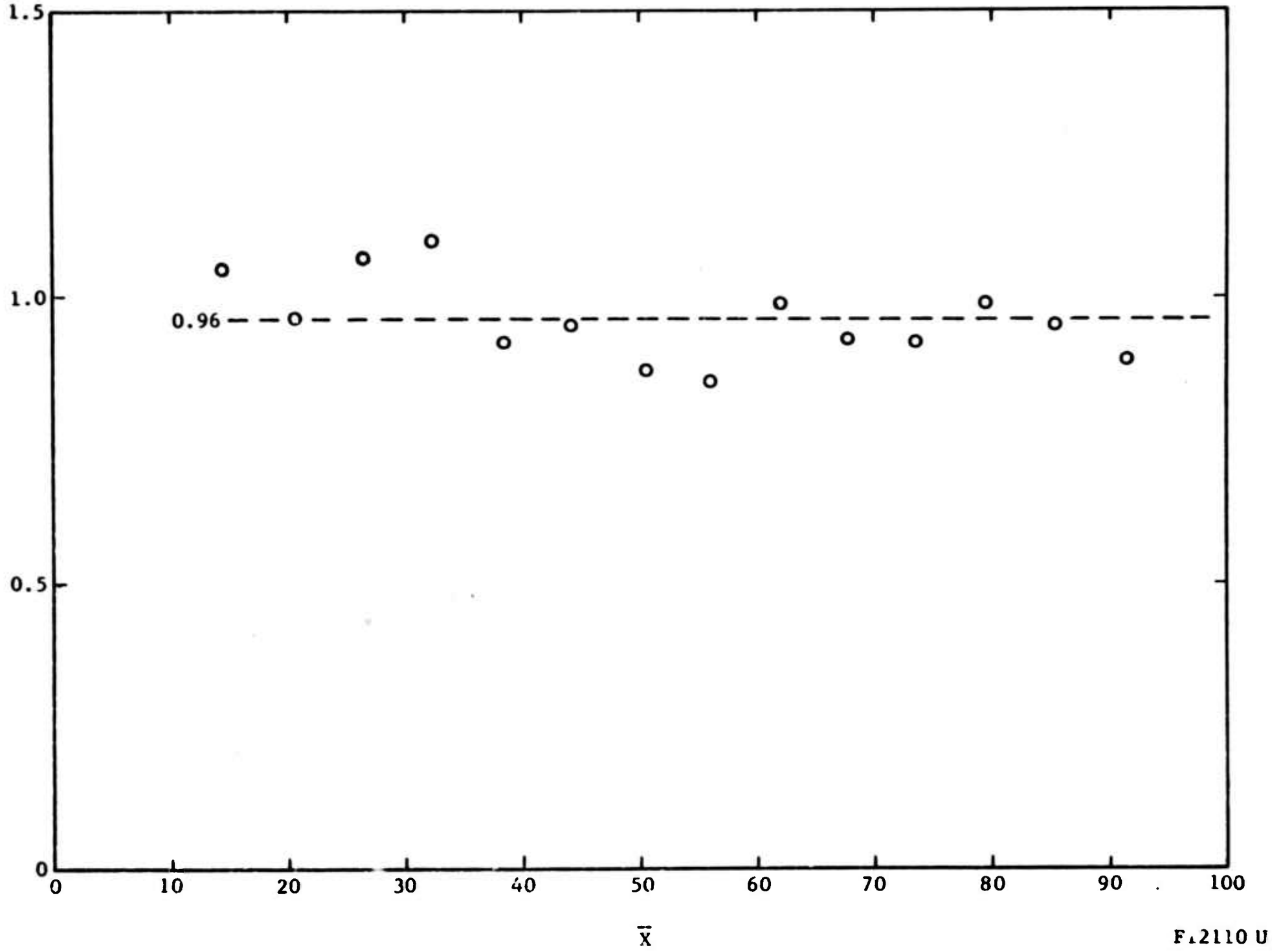

FIGURE 13. COINCIDENCE OF THE FRONT LOCATION AND THE POSITION OF MAXIMUM ZERO FREQUENCY

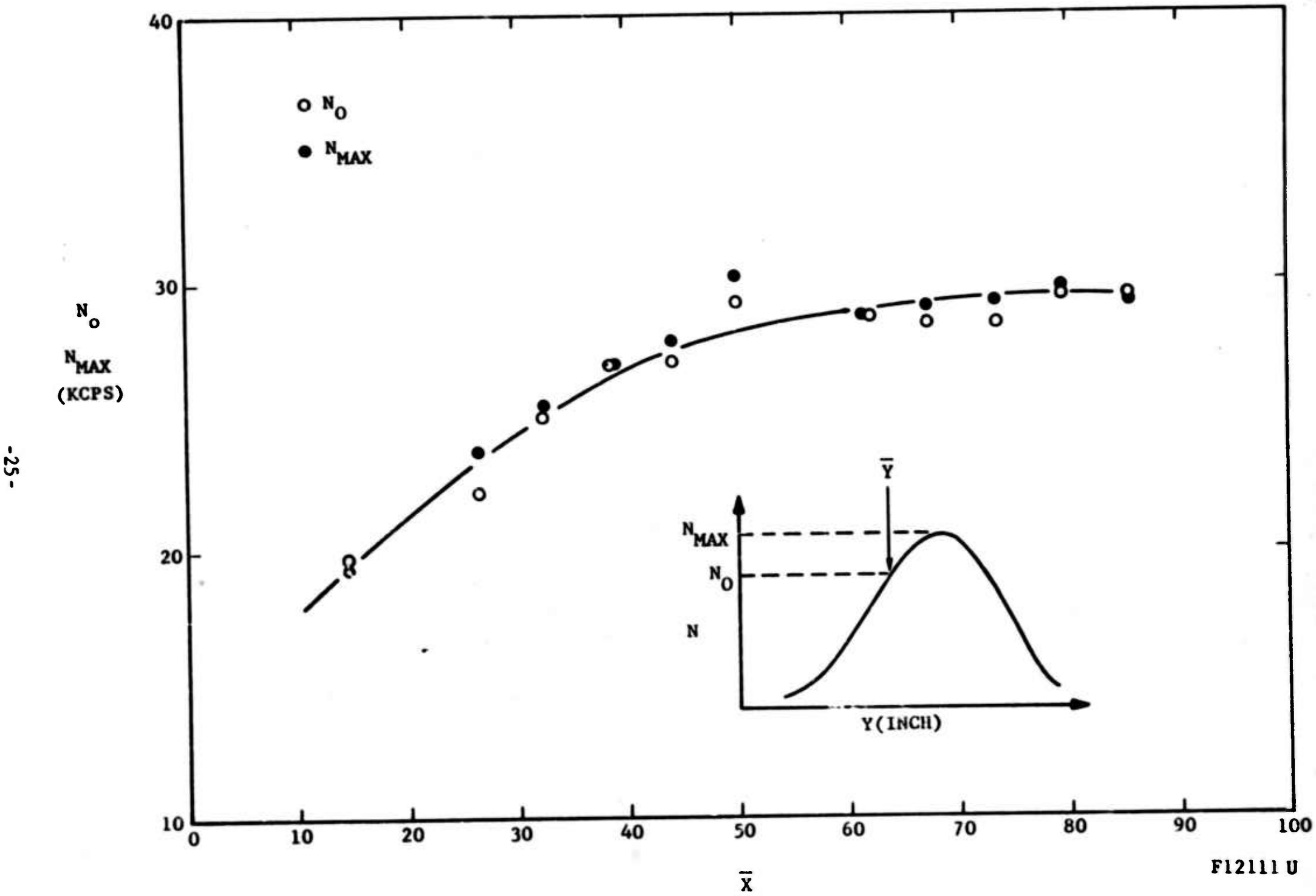

FIGURE 14. COINCIDENCE OF THE ZERO FREQUENCY N_o AT THE FRONT POSITION AND MAXIMUM FREQUENCY N_{max} AT EACH $\bar{X}$

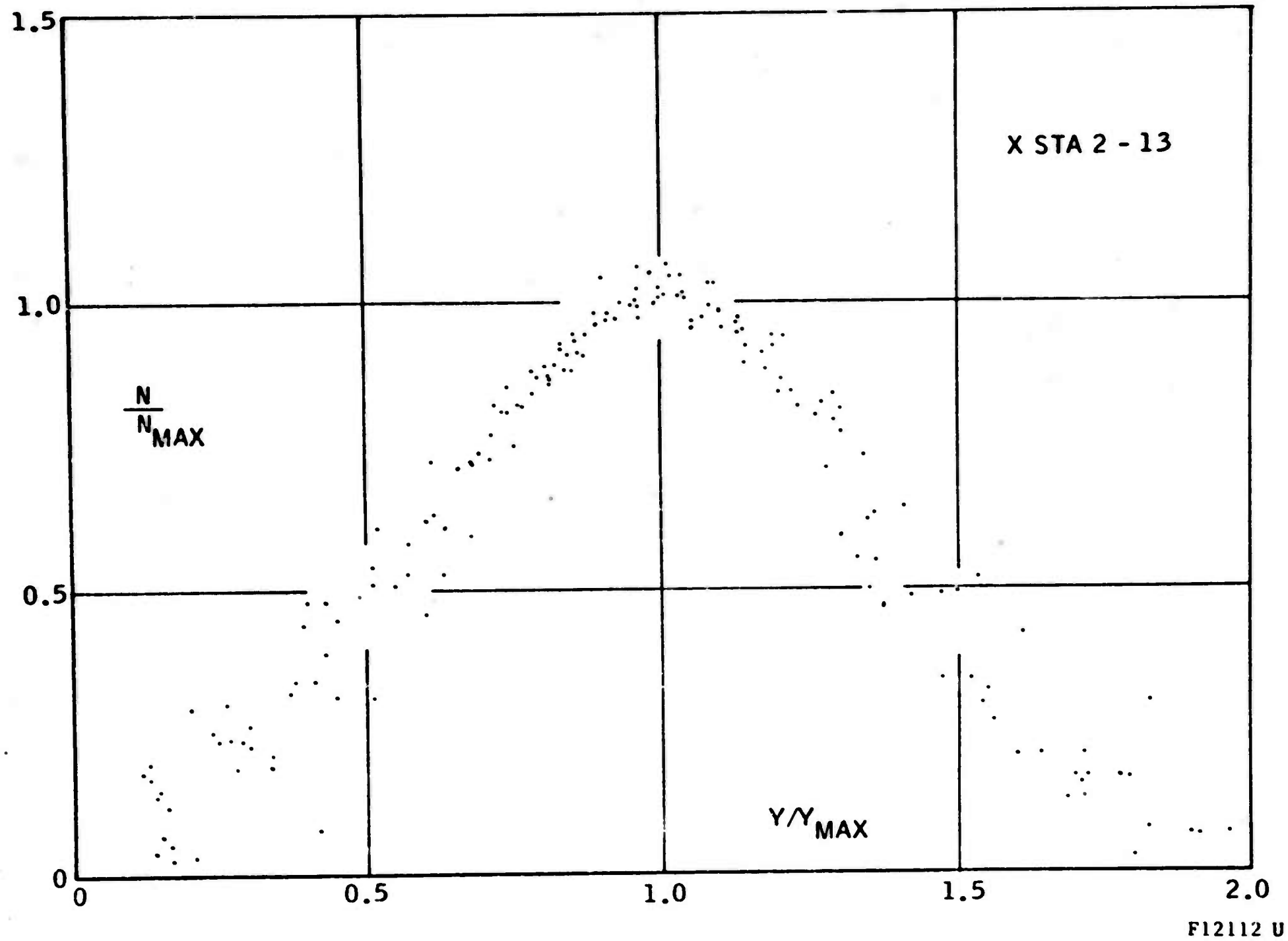

F12112 U

FIGURE 15. DISTRIBUTION OF ZERO FREQUENCY ABOUT THE FRONT LOCATION

manner suggested by Corrsin (Reference 1); the results are shown on Figure 16, normalized alternately with the local transverse scale L and the local wake radius $\bar{Y}$. It will be noted that the scaling of λ_F with these two parameters (which, of course, vary as $\bar{x}^{1/3}$, according to previous statements and the results of Reference 9) is at most tenuous, although some assemblance of such a proportionality appears towards the far end of the range investigated ($\bar{x} = 90$). A slight but still inadequate improvement is noted if $u(\bar{Y})$ (i.e., the mean flow velocity at the front position) is used* in Equation (4) in place of u_∞. In fact it would seem from Figure 17 that λ_F is probably constant along the wake, as illustrated by comparing λ_F with the (constant) $\sqrt{C_D A}$.

The apparent lack of an $\bar{x}$-dependence in λ_F is surprising because of the strength of dimensional arguments relating it to $L \sim \bar{x}^{1/3}$ (all other characteristic lengths such as Λ_u, Λ_T, σ, $\bar{Y}$ etc., scale with L) and to a lesser extent because such a dependence is apparently evident in ballistic-range experiments (References 5, 6, and 7). One possible explanation is that the front microscale is undergoing a relaxation process for $\bar{x} < 90$, of the type noted by Schapker (Reference 5), during which it remains constant.

In this connection it is relevant to ask whether the scale $\Lambda_F = u_\infty/N_o$ itself does not have a physical significance, especially because of the repeatability observed in measuring N_o. Since N_o is the "average number of zeros" Λ_F must have the meaning of an "average wavelength" which is, of course, $\pi/\sqrt{2}$ times larger than λ_F (cf Equation (4)). Almost exactly the same numerical difference between Λ_F and λ_F was also observed by Corrsin and Kistler who computed Λ_F from measurements of the average extent of the laminar and

*The rigor for using u_∞ in Equation (4) rests on Corrsin and Kistler's conclusion that "the mean velocity everywhere in the potential part of the flow must be constant and equal to that at infinity" (Reference 1, p. 15).

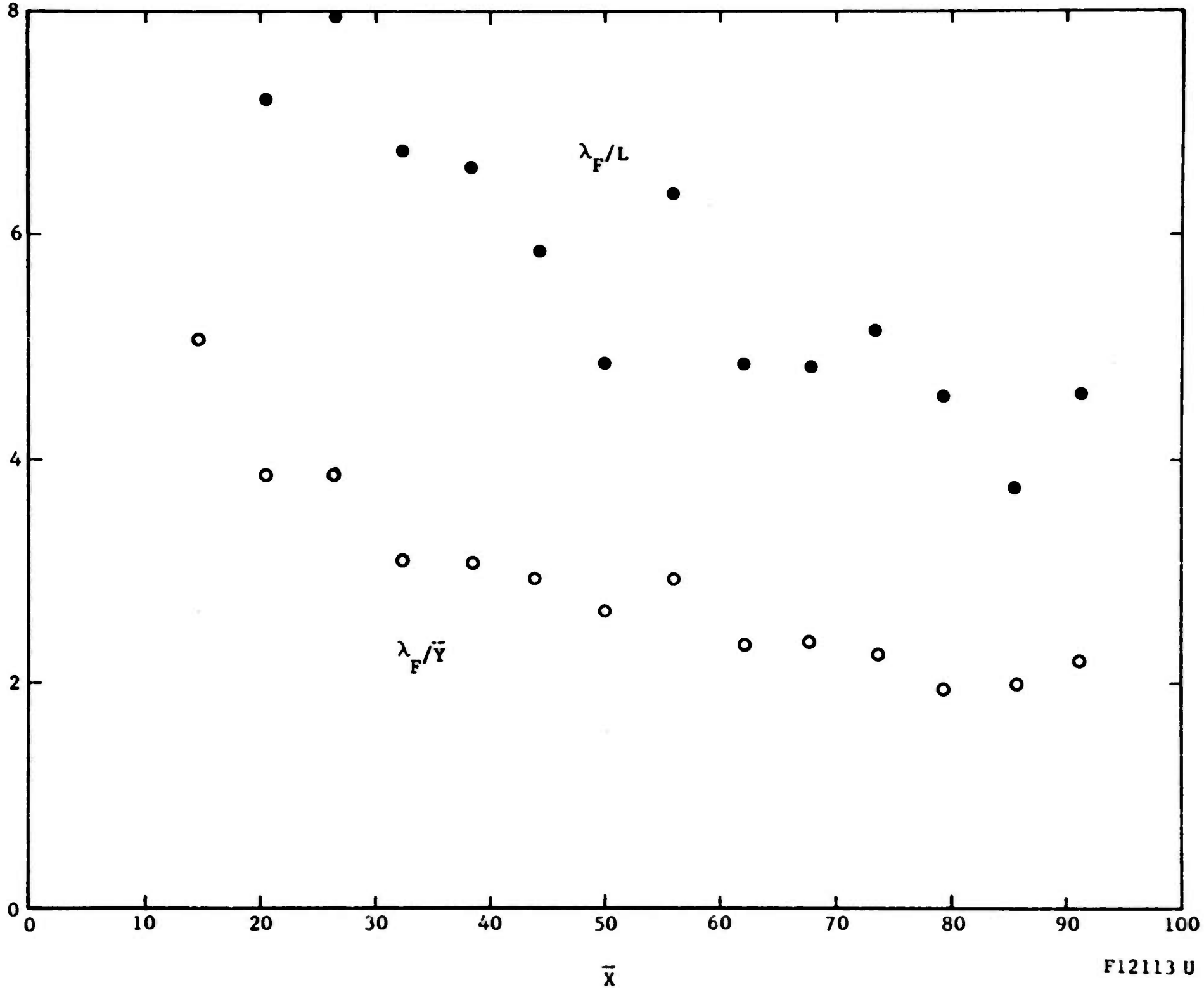

FIGURE 16. AXIAL VARIATION OF THE AUTOCORRELATION MICROSCALE OF THE TURBULENT FRONT

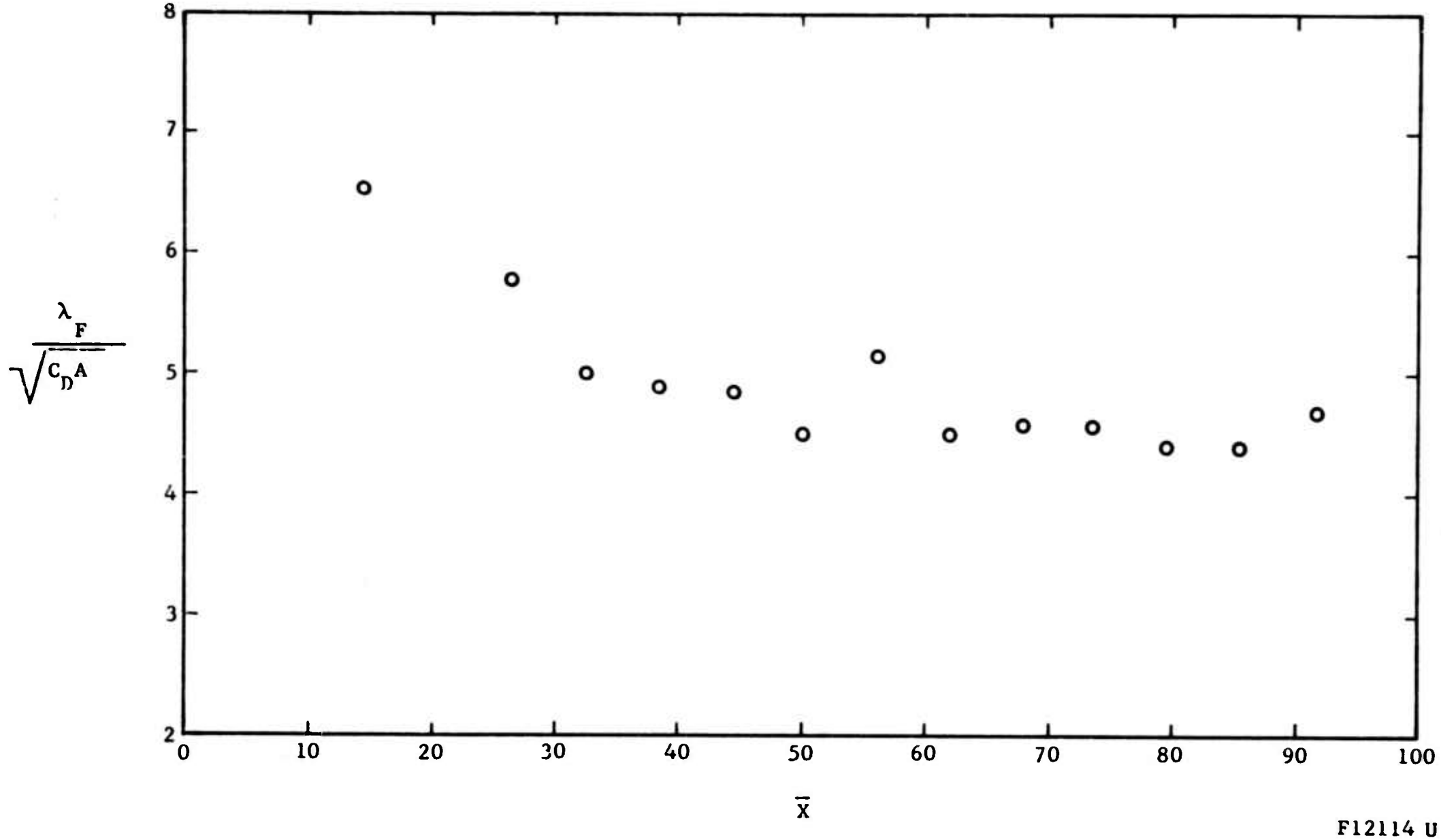

FIGURE 17. RELATION BETWEEN THE FRONT MICROSCALE AND THE WAKE MOMENTUM THICKNESS

turbulent regions at $Y = \overline{Y}$ (Reference 1, p. 26 to 28). This disparity was of seemingly minor importance in the latter instance because no additional phenomena were observed to give Λ_F a physical foundation (in the same manner, for example, as connecting the microscale to the Schmidt trigger output). In the present case additional phenomena featuring a wavelength Λ_F were observed; these will be described farther below.

6. DISCUSSION

6.1 EFFECT OF INTERMITTENCY ON FLUCTUATION MAGNITUDES

As a result of the preceding discussion and the generally accepted view of the turbulent front structure, the output of a stationary sensor in the intermittent region can be thought to consist of the bonafide turbulent signal superimposed on a "clipped" random signal due to the intermittency, which we shall henceforth call "pseudoturbulence". Much added effort is needed to study each of these two phenomena free from the influence of the other. In the meantime we shall, in this Section, examine phenomena indicating the presence of pseudoturbulence and use them to indicate their effect on the fluctuation magnitudes.

As shown in Appendix B the mean-square $\overline{(\Delta f)^2}$ of a variable which jumps by H across the front is

$$\overline{(\Delta f)^2} = H^2 \gamma (1 - \gamma) \qquad (7)$$

so that this amount is added to the overall hot-wire signal due to the intermittency (pseudoturbulence) alone. At the same time the overall signal also should be reduced by the familiar factor inversely proportional to γ to account for signal "loss" in the quiescent zones between turbulence zones. Psuedoturbulent effects for which the wire signal needs corrections consist therefore of two terms of opposing sign, as first brought up by Corrsin and Kistler (eg., (57) of Reference 1).

We now ask if the action predicted by Equation (7) is in any way visible in the present experiment. Although H is not known (and most likely depends on radial distance) the factor $\gamma(1 - \gamma)$ peaks at $\gamma = 0.5$, i.e., at the front position $\overline{Y}$. Another location where pseudoturbulent effects are visible should be the very edge of the wake ($\eta > 3$) where, according to Figure 7, the mean velocity and temperature have acquired the stream levels and where the front corrugations are too narrow to contain too many of the small eddies. To make the observations at these two locations easier, we recall that in compressible and heated flows the temperature and density jumps (i.e., the H values) across the front are certainly bigger than those of the velocity (Reference 13). The proper observable is therefore the temperature - in fact, it is the ratio $(\Delta T/T)/(\gamma-1)M^2(\Delta u/u)$ of the r.m.s. temperature to r.m.s. velocity fluctuations* properly normalized with the local Mach number (Reference 10). This quantity, plotted on Figure 18 versus radius for various axial positions, should be unity in a homogeneous turbulent gas without heat-transfer. In the figure both the maximum of $\gamma(1-\gamma)$ at $\eta \simeq 2$ and the precipitous increase of $(\Delta T/T)$ at large η are shown. In the latter case, (Figure 18 (b)) we see a mechanism driving especially large temperature fluctuations near the wake edge and it is submitted that these fluctuations are due to pseudoturbulence as anticipated above.

6.2 EFFECT OF INTERMITTENCY ON FLUCTUATION SPECTRUM

In addition to the effect on the fluctuations magnitude, effects on their spectra suspected to be due to pseudoturbulence have been observed.

As indicated in Reference 10, the longitudinal spectra of the turbulent fluctuations of wake density and axial velocity have exhibited a marked intensity prominence at frequencies ranging from about 30 to 50 kilocycles per second. It was concluded, in that reference, that this "peak" in the spectra was due to the front corrugations being organized into a weakly periodic structure. The periodicity was found to be most intense immediately

*Here γ is the ratio of specific heats.

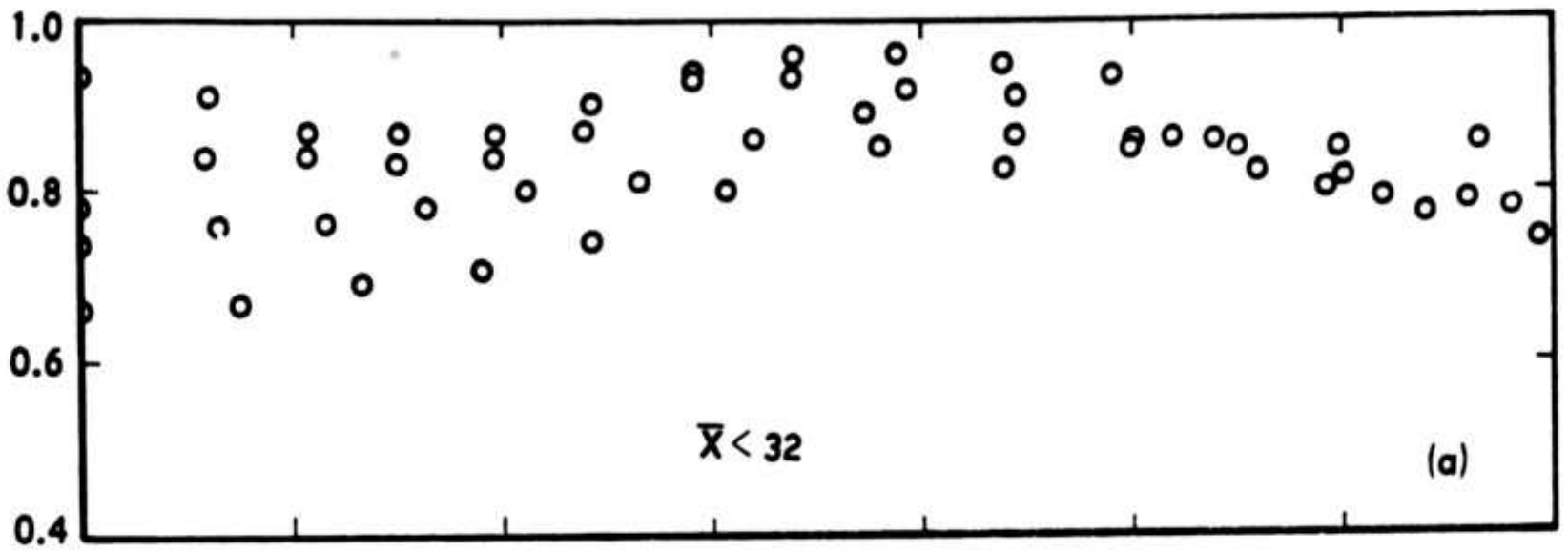

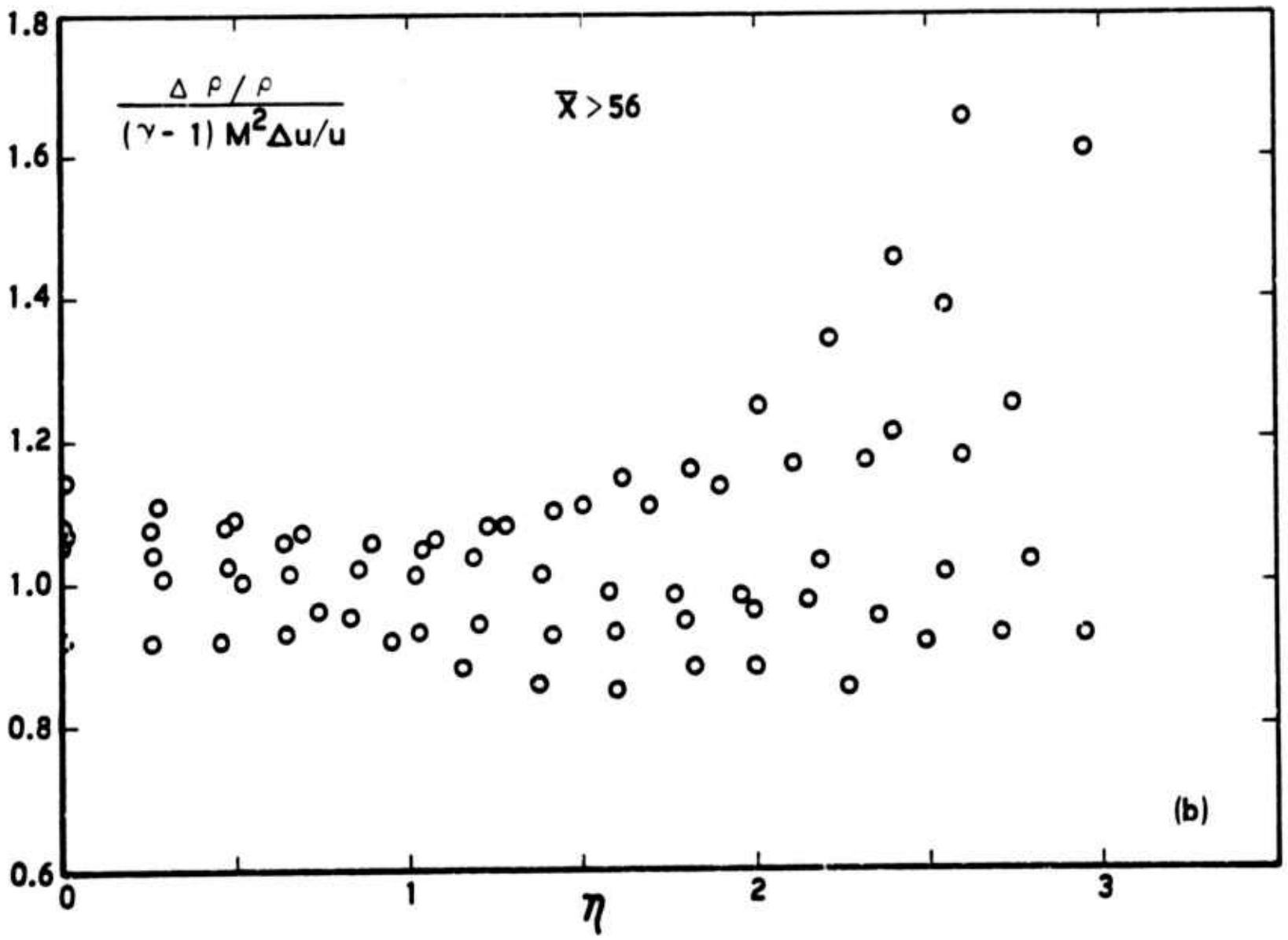

FIGURE 18. TEST OF THE "STRONG REYNOLDS ANALOGY" FOR THE RELAXING (TOP) AND THE SELF-PRESERVING WAKE (BOTTOM).

after transition to turbulence, decaying so that it was barely discernible at $\bar{X} = 90$. If this periodicity was due to the pseudoturbulence it is natural to expect that it would surface clearly if the pseudoturbulent spectrum could be measured separately from that of the overall signal. The separation of the two types of spectra is not an easy matter, but a fair picture of the situation is given by the output spectrum of the Schmidt trigger (i.e., of the lower traces in the photographs of Figure 5). Figure 19 shows raw data of the trigger output spectra compared with the overall hot-wire spectra (i.e., the top traces in Figure 5). Both spectra show clearly the peak located at the same frequency.

These observations suggest that the front is organized into a periodic structure, and can be further discussed with the aid of a rudimentary model, as done previously by Bradbury (Reference 14) and as shown on Figure 20. For purposes of illustration the irregular shape of the corrugated front is replaced by a periodic structure in the form of adjoining half-circles. The wire signal in space or time then consists of a series of rectangular waves with superposed turbulent fluctuations; the latter is very much in accord with the observations (see Figure 5) although in the present discussion we imagine that the rectangular waves are also periodic. It is natural to suppose, as shown inFigure 20, that the spectrum of such a signal is somehow decomposable into the spectrum of the turbulence itself and that of the rectangular waves produced by the corrugations. The turbulence spectrum be what it may, the pseudo-turbulent spectrum due to the rectangular waves, discussed in Appendix B, has a fundamental at the characteristic front wavelength and weakening harmonics at integral values of the fundamental. As shown in Figure 20, therefore, the spectrum combining the turbulence and intermittency phenomena should show a peak for a large portion of the radius between the axis and the wake boundary. This is, in fact, observed in Figures 42 through 63, in Reference 10. Naturally, the observed peak due to the pseudoturbulence is "weak" in the sense that its Fourier components are

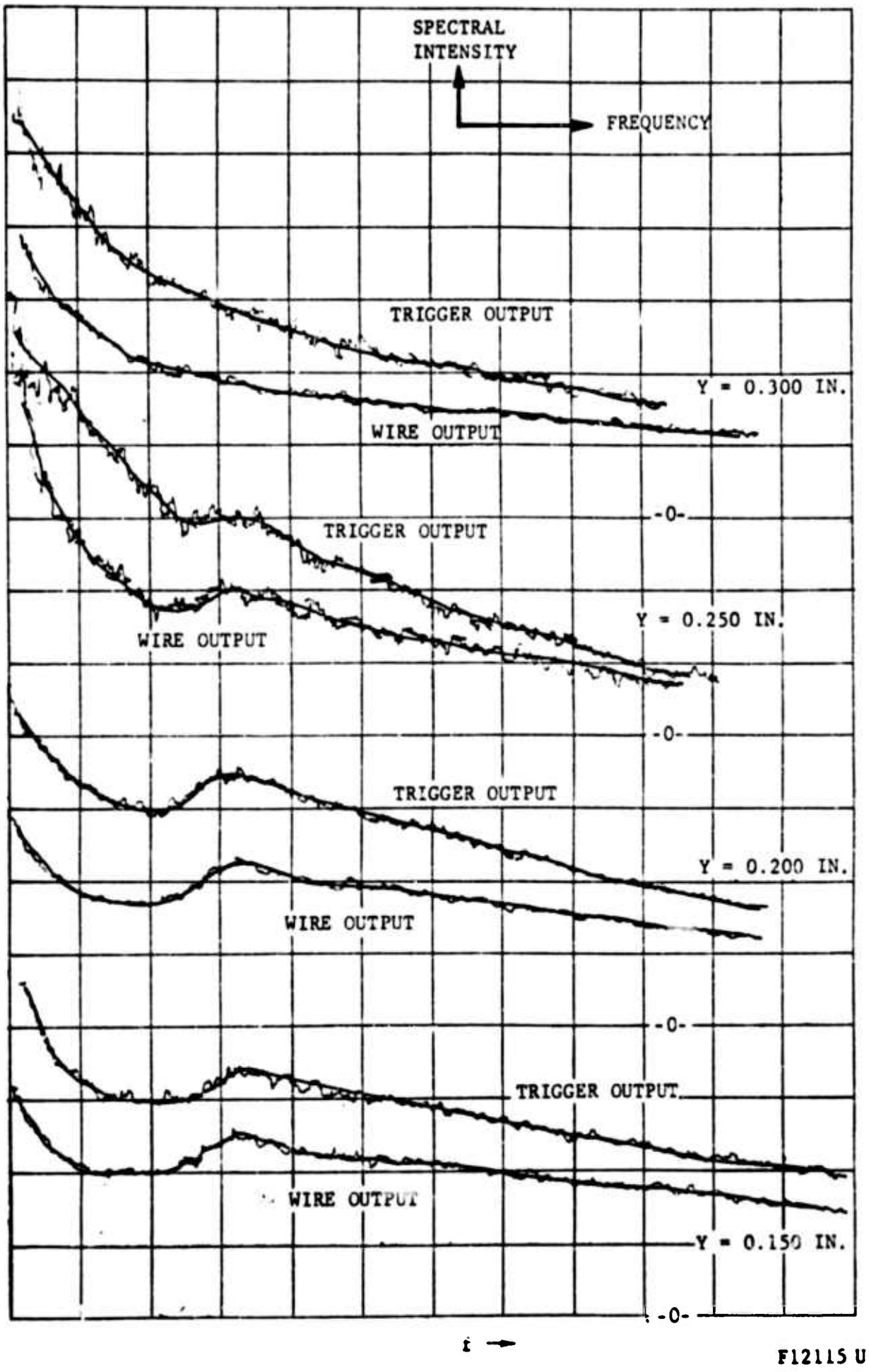

FIGURE 19. QUALITATIVE COMPARISON OF THE SCHMIDT TRIGGER OUTPUT SPECTRA WITH THE HOT-WIRE OUTPUT SPECTRA

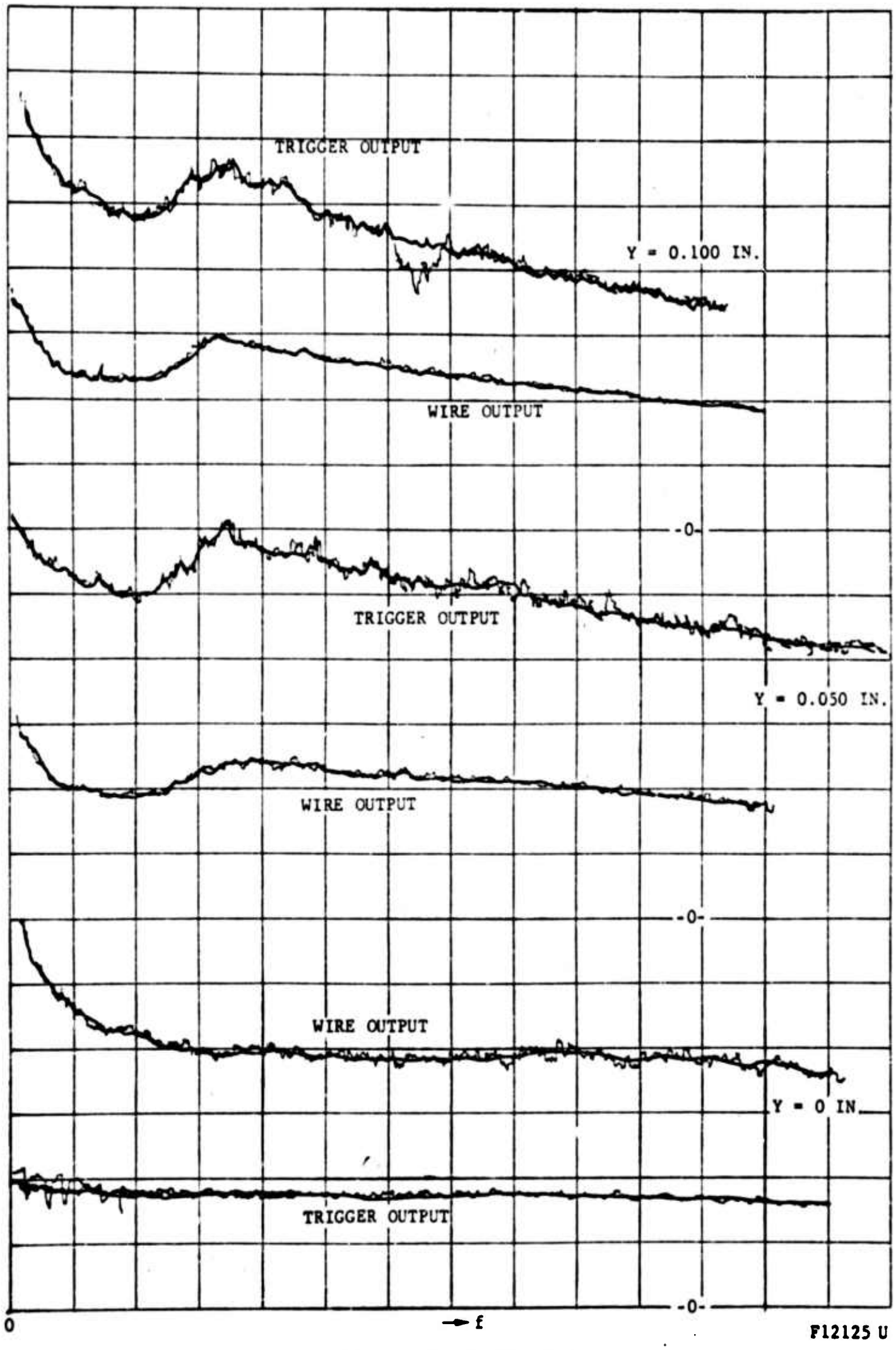

FIGURE 19. (CONTINUED)

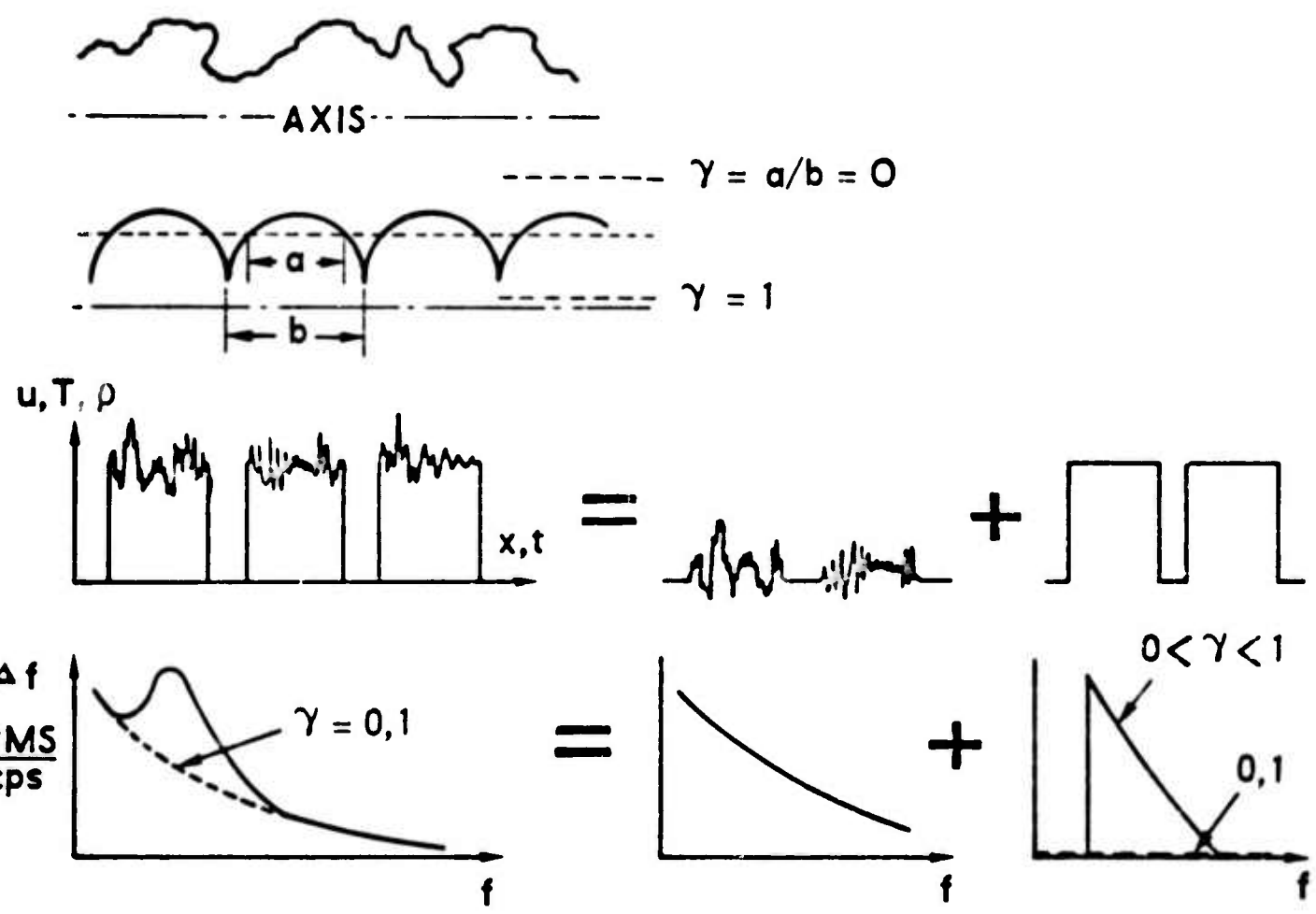

F09819 U

FIGURE 20. EFFECT OF INTERMITTENCY ON THE SPECTRUM OF A TURBULENT WAKE

in reality dispersed considerably. In fact the Schmidt trigger output spectrum of Figure 19 looks much like the "Poisson" spectrum observed at the same output by Corrsin (Reference 1) but with a peak superimposed. We conclude that the periodic structure is indeed tenuous, perhaps appearing and disappearing cyclically as suggested by Townsend (Reference 2) and Grant (Reference 15).

If the fluctuation concentration (the "peak") in the hot-wire output spectrum is thus identifiable with a periodic component of the pseudo-turbulence, it is worthwhile to test Equation (7) for that component alone, just as (7) was tested in Figure 18 for the entire pseudoturbulent signal. Figure 21 shows the density fluctuation intensity variation with radius for a narrow (1 kcps) fluctuation passband about a frequency at 35 kcps, that is in the immediate vicinity of the pseudoturbulence peak. The maximum of this curve is very close to $\eta = 2$ where the maximum also occurs in the $\gamma(1-\gamma)$ curve. For comparison, the mean-square density fluctuation integrated over all frequencies is also plotted; its own maximum occurs, at this case, around $\eta = 1.5$, that is closer to the radial location of the maximum shear region, as already discussed in Reference 10. It appears to some degree, at least, that the behavior of pseudoturbulent "periodicity" is described by the rough argument given previously.

6.3 WAVELENGTH OF THE TURBULENT FRONT

The periodicity detected in the wire signal and its clipped (Schmidt trigger) counterpart has a wavelength $u(\bar{Y})/f_T$ where f_T is the peak frequency in the spectra of Figure 19. We have also detected another wavelength $u(\bar{Y})/N_o$ where N_o is the frequency of zeros at the front location; this is, as explained in Section 5.2, $\pi/\sqrt{2}$ times the front microsale. We ask what the connection between these two wavelengths is, and what is their magnitude related to other characteristic lengths in the wake.

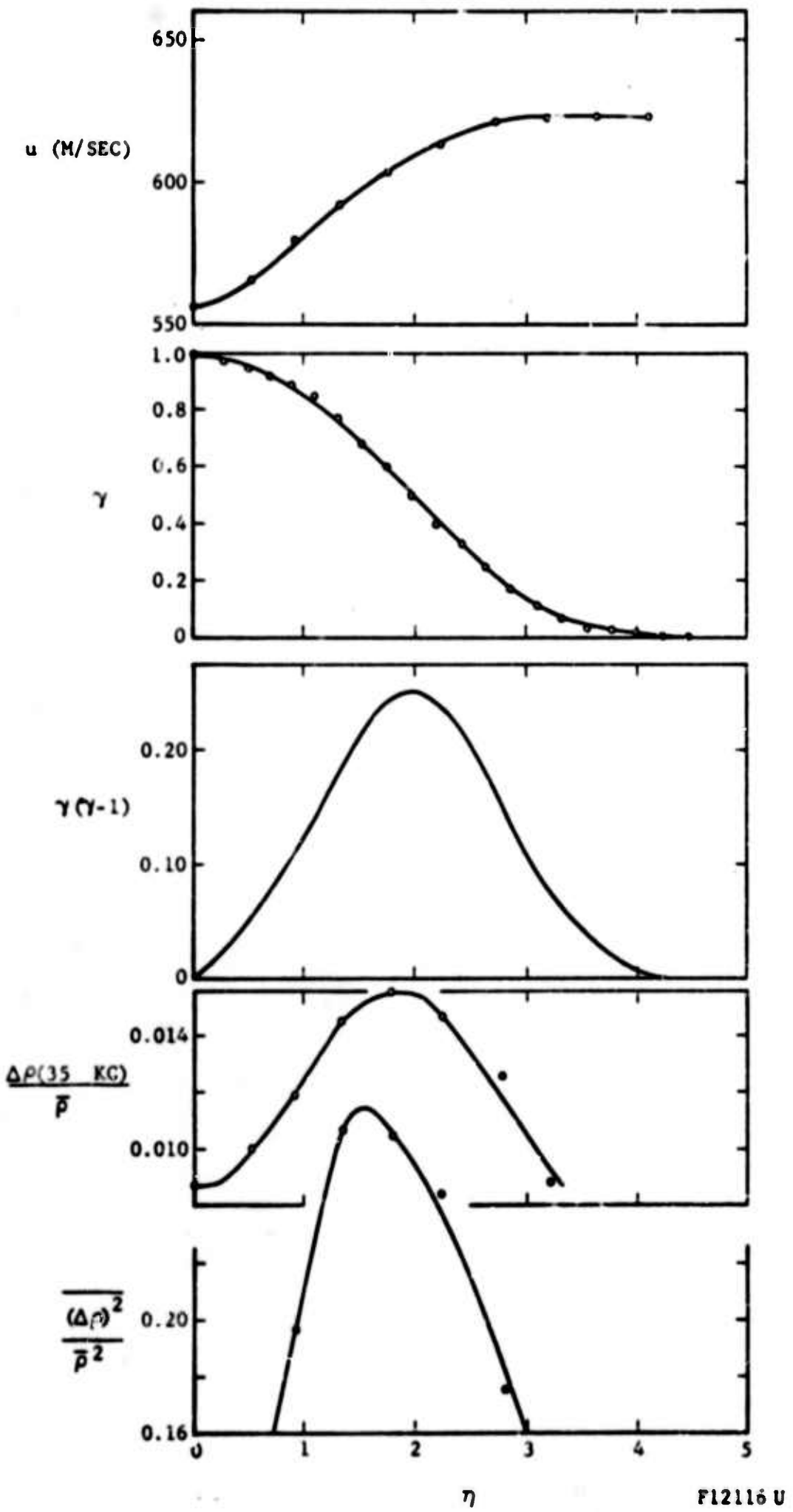

FIGURE 21. RADIAL VARIATION OF THE 35-KILOCYCLE FOURIER COMPONENT OF THE DENSITY SPECTRUM (FOURTH FROM TOP) SHOWING TENDENCY TO FOLLOW THE PSEUDOTURBULENT (THIRD FROM TOP) RATHER THAN THE INTEGRATED TURBULENT INTENSITY (BOTTOM)

Figure 22 plots these two wavelengths, which are seen to be about equal farther along the wake; this equality could in anyway be predicted earlier since N_o and f_T were found to be about equal. Nc explanation exists for the differences below $\bar{X} = 30$, however. A value $\Lambda_F \equiv u(\bar{Y})/N_o = u(\bar{Y})/f_T = 9 \pm 2$ seems to prevail. Added commentary on Λ_F will be made further below.

6.4 COMPARISON WITH OTHER EXPERIMENTS

It would be interesting to compare, whenever possible, the present results with those obtained in other intermittency measurements. In low-speed flows, for example, Corrsin and Kistler (Reference 1) have observed that γ is distributed $(Y - \bar{Y})/\sigma$ in a manner independent of the type of flow (wake, jet or boundary layer). This "universal" curve agrees well with the present results, as shown on Figure 23. This agreement is, of course, fully expected since γ, σ and $\bar{Y}$ are in essence moments of each other. It is hardly surprising, therefore, that measurements subject to added natural aberrations, such as the ballistic-range measurements of Levensteins and Krumins (Reference 6) show equally good agreement.

It is much more significant to relate the intermittency behavior to the transport of momentum across the turbulent flow. Thus the spreading rates of $\bar{Y}$ and σ, as Corrsin demonstrated, follow the dependence of the flow scale L on distance $\bar{X}$ and are thus dependent on the type of flow at hand. It has already been seen in Reference 9 that in the present wake $L \sim \bar{X}^{1/3}$, and in Figures 8 and 9 of this report the relationship $\sigma \sim \bar{Y} \sim L \sim \bar{X}^{1/3}$ is fully verified; in Townsend's cylinder wake (Reference 12) $\sigma \sim \bar{Y} \sim L \sim \bar{X}^{1/2}$ as expected.

Table III shows a numerical comparison of the present results with those available from low-speed experiments; the significance of the transverse scale L is clearly demonstrated in this table. It should be noted that the position $\bar{Y}$ of the front and the turbulent macroscales Λ_u (the longitudinal velocity scale) and Λ_T (the longitudinal temperature scale) and perhaps the front "macroscale" Λ_F, seem to be universally constant for

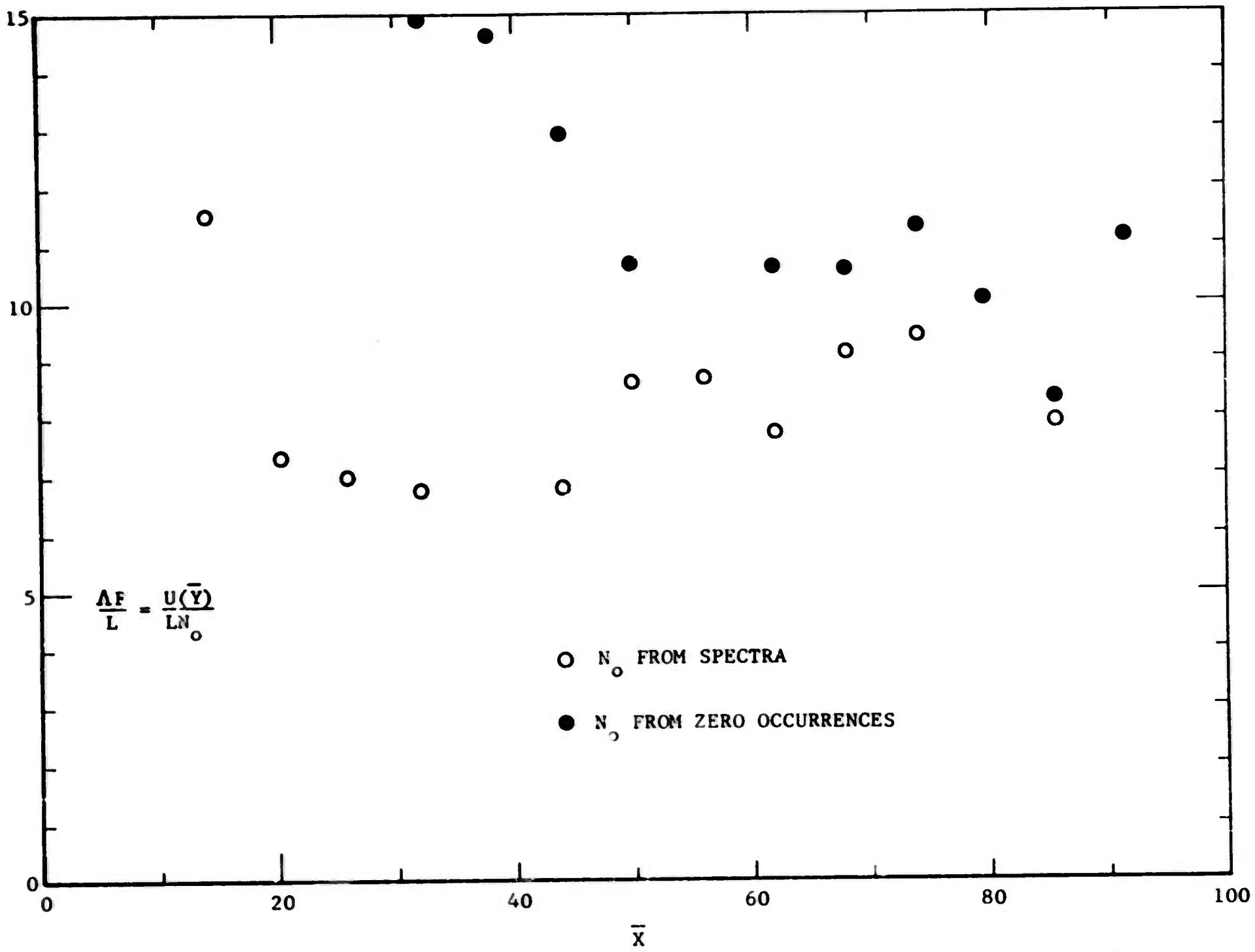

FIGURE 22. WAVELENGTH OF THE TURBULENT FRONT NORMALIZED WITH THE TRANSVERSE SCALE, AS DEDUCED FROM TWO INDEPENDENT MEASUREMENTS

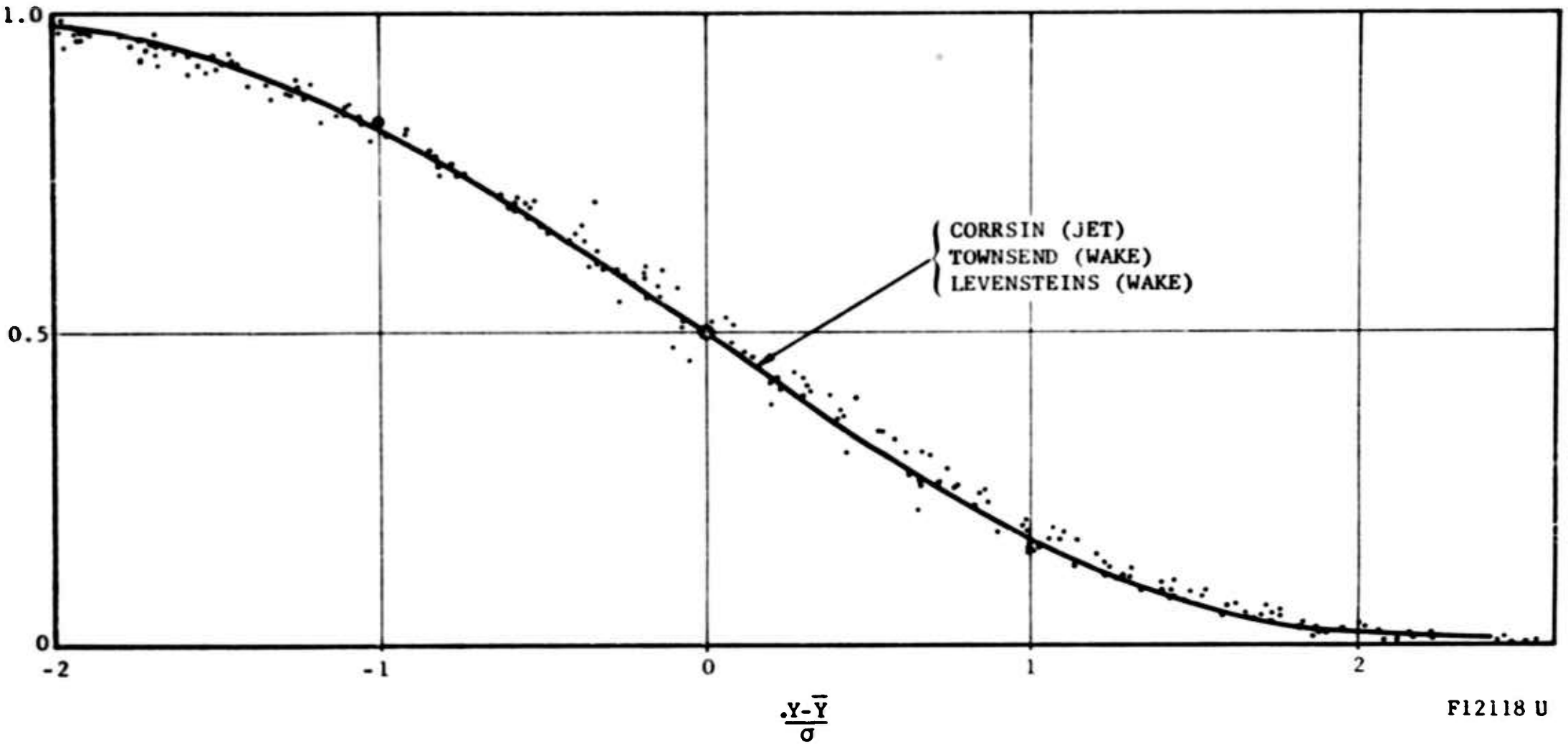

FIGURE 23. COMPARISON OF THE INTERMITTENCY FACTOR RADIAL DISTRIBUTION WITH OTHER EXPERIMENTS

TABLE III. COMPARISON WITH OTHER EXPERIMENTS

	Present Work (Wake)	Townsend (Wake)	Grant (Wake)	Bradbury (Jet)
$\overline{Y}/L$	2.1	2.1	2.1	2.0
σ/L	0.87	0.80	0.80	0.44
$\sigma/\overline{Y}$	0.41	0.38	0.38	0.22
$\Lambda_u/\overline{Y}$	0.5*	0.5	0.5	0.55
Λ_u/L	1*	1.06	1.06	0.92***
Λ_u/Λ_T	0.5-1**	---	---	0.58***
λ_F/L	4.6	---	---	---
Λ_F/L	9 ± 2	---	---	---
$\eta(\tilde{u} = .01)/L$	3.28	---	---	---
$\eta(\gamma = .01)/L$	4.5	---	---	---

*bad scatter (from Reference 10)

**0.5 on axis, 1 near edge (from Reference 10)

***Corrsin & Uberoi data (Reference 19)

different types of flow; the standard deviation differs for the jet and, as Townsend (Reference 2) points out, for the boundary layer as well. This difference has been attributed by Gartshore (Reference 16) to differences in the effective turbulence Reynolds number R_T among such flows. His exact expression, put into the present nomenclature reads

$$\frac{\sigma}{L} = \frac{2.97}{\sqrt{R_T}} \qquad (8)$$

which gives $\sigma/L = 0.83$ for the $R_T = 12.8$ found in the present experiment (Reference 9). Note that a slight difference between Equation (8) and Gartshore's formula (p. 97 of Reference 16) exists because the transverse scale L is about 22% smaller than Gartshore's L_o which is the flow "half radius".

The possibility of a periodic front has been well established by Grant (Reference 15) and Keffer (Reference 17); Townsend (Reference 2) has made calculations of possible front indentations based on stability arguments and finds that such waves have a length 6.3L. Recent experiments in a highly heated jet (Reference 18) have disclosed a similar periodicity in its interface with a wavelength of about 8L. We can therefore conclude that (a) a weak periodicity of the front structure seems to exist, (b) the wavelength lies around 9L and (c) the periodicity affects the spectra sensed by the hot-wire.

As previously noted, no stretches of ambient (irrotational) fluid was found on the wake axis, where $\gamma = 1$ always. This is in contrast with the results and Gibson (Reference 3) and Baldwin (Reference 4), and a tentative explanation of the difference can be given by combining Gartshore's results (Reference 16) with a brief critique made by Behrens (Reference 20) of low-speed wake experiments. Behrens observed that the turbulent Reynolds number R_T for axi-symmetric bodies is not constant but varies with bluntness, from about 1 for very blunt (say,

disks normal to the flow) to about 10 for very slender bodies; at the latter extreme R_T is about equal to that for two-dimensional wakes (in the present wake $R_T = 12.8$ was obtained, very close to the value of 12.7 for cylinders at low speeds). Further along the scale one can obtain R_T as high as 30, 40 or 50 for jets. As illustrated on Figure 24, Equation (8) predicts large differences in the standard deviation σ for flows of very different R_T. On one end of the scale, the standard deviation for jets is small compared to the flow width. For the present experiment ($R_T = 12.8$) σ has increased to the point where the axis barely escapes an occasional brush with the external flow. For blunt axisymmetric bodies, however, the "wrinkle amplitude" represented by σ should become so large (it is $\sigma/L \simeq 3$ at $R_T = 1$; in the present work we have $\sigma/L = 0.87$) that the front corrugation depth reaches and exceeds the wake axis. In the extreme, therefore, the wake would not resemble a straight cylinder with rough surface but rather a cylinder with grossly ondulating axis. Gibson's own photograph of his wake (Reference 3) seems to confirm this very description.

A comparison can finally be made with the hypervelocity observations in ranges as summarized inFigure 11 of Reference 6, if we put $\delta = 2\bar{Y}$ in Figure 9,

$$\frac{\sigma}{\delta} = \frac{\sigma}{2\bar{Y}} = 0.20$$

The agreement is poor, and is definitely due to the manner in which δ is defined and measured in the range experiments (Reference 5,6) and especially the possibility of underestimating σ in the latter. This under-estimation must be in turn due to the inability to detect the front "valleys", as mentioned in the Introduction.

The comparison of the microscale is difficult again because the range experiments have no way of relating λ_F with L or $\sqrt{C_D A}$ where the latter

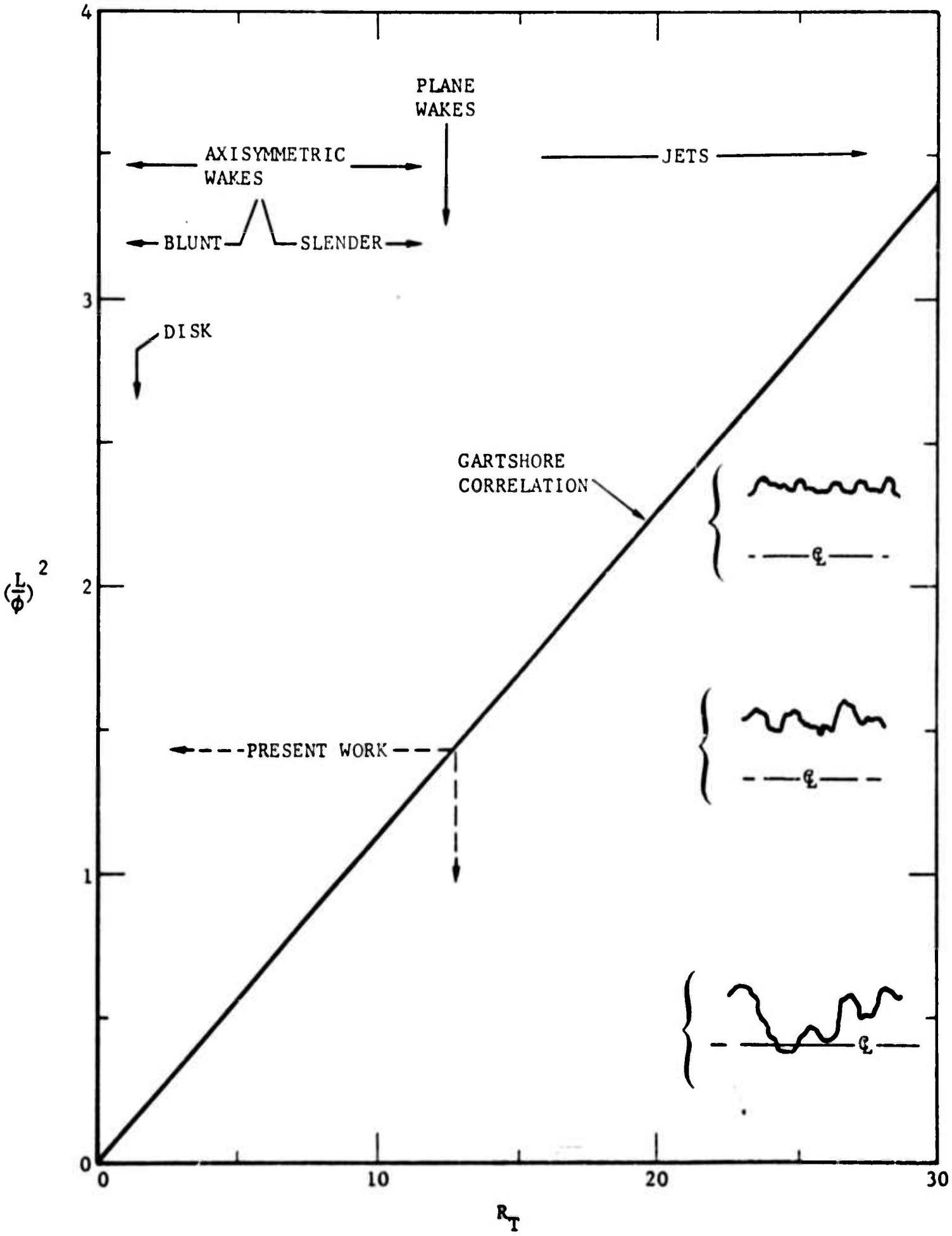

FIGURE 24. RELATION BETWEEN STANDARD DEVIATION AND TRANSVERSE SCALE FOR FREE TURBULENT FLOWS AS A FUNCTION OF THE TURBULENT REYNOLDS NUMBER

refers to the wake alone. However, some semblance of the dependence $\lambda \sim \bar{X}^{1/3}$ is seen in Figure 13, Reference 6.

7. CONCLUSIONS

We draw the following conclusions from the results presented above:

(1) A fully turbulent region exists about the axis of the wake; this region is very narrow in extent (compared to the wake diameter) in the self-preserving region. No occurrence of irrotational flow on the axis, of the type observed by Baldwin and Gibson, was seen.

(2) The wake front $\bar{Y}$ is located at $\eta = 2.1$; the wake "diameter" $2\bar{Y}$ thus is about 4.2L where L is the transverse scale. The standard deviation of the front corrugations $\sigma = 0.87L$. These results are in very good agreement with low-speed wake results but in poor agreement with ballistic range results.

(3) The distribution of γ about the front position (i.e., with $(Y - \bar{Y})/\sigma$) is Gaussian in character and identical with all similar variations reported so far, apparently including ballistic range (hypervelocity) experiments.

(4) The intermittency "radius" of the wake is located at $\eta(\gamma = 0.01) \simeq 4.5$, contrasted with $\eta\ (\tilde{T} = 0.01) = 3.65$ and $\eta(\tilde{u} = 0.01) = 3.28$, the "temperature" and "velocity" radius respectively.

(5) The longitudinal autocorrelation microscale λ_F of the front does not seem to scale well with L in the range of $\bar{X}$ studied, although at large $\bar{X}$, $\lambda_F \simeq 4L$.

(6) A weak periodicity in the front geometry was noted with a wavelength $\Lambda_F = 9L \pm 2L$. In the spectral sense this periodicity affects the spectra of turbulence within the wake itself.

The characteristic lengths of the wake are shown on Figure 25.

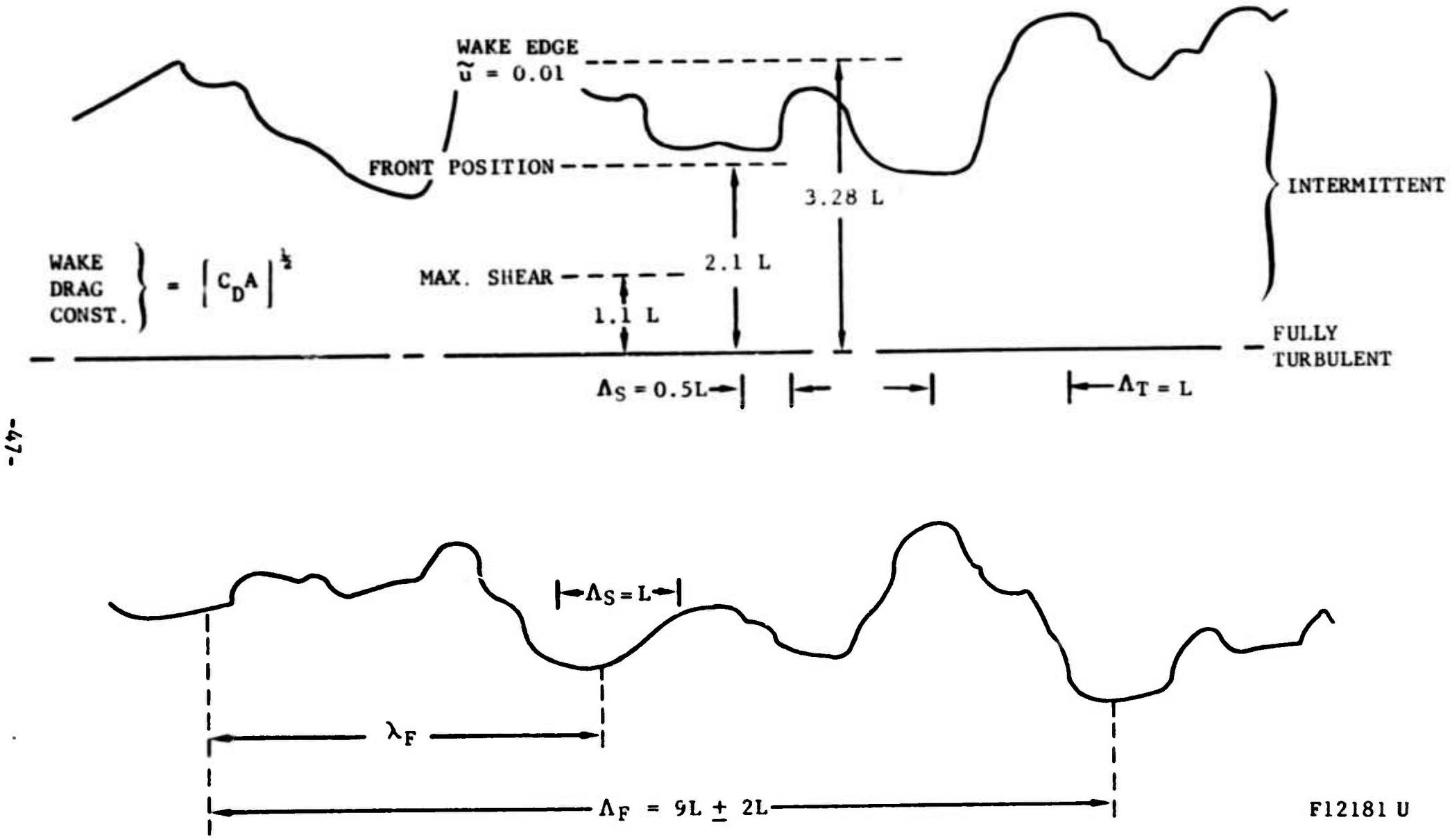

FIGURE 25. SCHEMATIC DIAGRAM OF THE WAKE MODEL COMPOSED FROM THE PRESENT EXPERIMENTAL RESULTS

REFERENCES

1. Corrsin, S. and Kistler, A. L., "Free-Stream Boundaries of Turbulent Flows," NACA Report 1244, 1955.
2. Townsend, A. A., "The Mechanism of Entrainment in Free Turbulent Flows," J. Fluid Mech., Vol. 26, Part 4, pp. 689-715, 1966.
3. Gibson, C. H., Lin, S. C., and Chen, C. C., Measurements of Turbulent Velocity and Temperature Fluctuations in a Wake of a Sphere, AIAA Paper No. 67-20, New York, New York, January 1967.
4. Hwang, N.H.C. and Baldwin, L. V., "Decay of Turbulence in Axi-Symmetric Wake," ASME Paper.
5. Shapker, R. L., Statistics of High-Speed Turbulent Wake Boundaries, AIAA Preprint 65-808, San Diego, California, 13 December 1965.
6. Levensteins, Z. J. and Krumins, M. V., "Aerodynamic Characteristics of Hypersonic Wake," AIAA J., Vol. 5, No. 9, p. 1596, Sept. 1967.
7. Knystautas, R., "The Growth of the Turbulent Inner Wake behind a 3-inch Diameter Sphere," C.A.R.D.E. TR 488, January 1964.
8. Fox, J., Webb, W. H., Jones, B. G., and Hammitt, A. G., "Hot-Wire Measurements of Wake Turbulence in a Ballistic Range," AIAA Journal, Vol. 5, No. 1, p. 99, 1967.
9. Demetriades, A., "Mean Flow Measurements in an Axisymmetric Compressible Turbulent Wake," Philco-Ford Corporation Report U-3978, Newport Beach, California, March 1967; also to be published in AIAA Journal, 1967.
10. Demetriades, A., "Turbulence Measurements in an Axisymmetric Compressible Wake," Philco-Ford Report No. UG-4118, Newport Beach, California, August 1967.
11. Bradbury, L.J.S., A Single Circuit for the Measurement of the Intermittency Factor in a Turbulent Flow, Aeronautical Quarterly, Vol. 15, p. 281, 1964.
12. Townsend, A. A., The Structure of Turbulent Shear Flow, Cambridge University Press, 1956.

13. Meyer, E. and Divoky, D., "Correlation of Intermittency with Preferential Transport of Heat and Chemical Species in Turbulent Shear Flows," AIAA Journal, Vol. 4, No. 11, p. 1995, 1966.

14. Bradbury, L.J.S., "The Structure of a Self-Preserving Turbulent Plane Jet," Journal of Fluid Mechanics, Vol. 23, Part 1, pp. 31-64, 1965.

15. Grant, H. L., J. Fluid Mech. Vol. 4, p. 149, 1958.

16. Gartshore, I. S., J. Fluid Mech., Vol. 24, p. 89, 1966.

17. Keffer, J. F., J. Fluid Mech., Vol. 22, p. 135, 1965.

18. Demetriades, A. and Doughman, E. L., "Mean and Intermittent Flow in a Self-Preserving Plasma Jet," Philco-Ford Corp., Newport Beach, Calif., (to be published).

19. Corrsin, S. and Uberoi, M. S., Further Experiments on the Flow and Heat Transfer in a Heated Turbulent Jet, NACA TR 998, Washington, D.C., 1950.

20. Behrens, W., "A Comparison of Incompressible Turbulent Wake Flow Investigations," GALCIT Hypersonic Research Project IM No. 15, Pasadena, Calif., July 1, 1963.

21. Menzel, D. H. (Editor), Fundamental Formulas of Physics, Vol. I, Dover Publications, Inc., New York, 1960, p. 74.

13. Meyer, E. and Divoky, D., "Correlation of Intermittency with Preferential Transport of Heat and Chemical Species in Turbulent Shear Flows," AIAA Journal, Vol. 4, No. 11, p. 1995, 1966.

14. Bradbury, L.J.S., "The Structure of a Self-Preserving Turbulent Plane Jet," Journal of Fluid Mechanics, Vol. 23, Part 1, pp. 31-64, 1965.

15. Grant, H. L., J. Fluid Mech. Vol. 4, p. 149, 1958.

16. Gartshore, I. S., J. Fluid Mech., Vol. 24, p. 89, 1966.

17. Keffer, J. F., J. Fluid Mech., Vol. 22, p. 135, 1965.

18. Demetriades, A. and Doughman, E. L., "Mean and Intermittent Flow in a Self-Preserving Plasma Jet," Philco-Ford Corp., Newport Beach, Calif., (to be published).

19. Corrsin, S. and Uberoi, M. S., Further Experiments on the Flow and Heat Transfer in a Heated Turbulent Jet, NACA TR 998, Washington, D.C., 1950.

20. Behrens, W., "A Comparison of Incompressible Turbulent Wake Flow Investigations," GALCIT Hypersonic Research Project IM No. 15, Pasadena, Calif., July 1, 1963.

21. Menzel, D. H. (Editor), Fundamental Formulas of Physics, Vol. I, Dover Publications, Inc., New York, 1960, p. 74.

APPENDIX A

THE WEB-V' COMPUTER PROGRAM

This program is designed to process intermittency data in wake-like turbulent flows. Its primary inputs are the distribution of intermittency factor γ (gamma) and zero-occurrence frequency N, with secondary inputs from the WEB-I and WEB-V programs.

Referring to the procedural diagram of Figure A-1, a number of discrete points γ at each Y_γ are inputed at each XSTATION. A polynomial γ (Y_γ) is produced by the computer to curve-fit this distribution (usually between 6th and 8th degree polynomials). The curve-fitting process consists of searching for a minimum in the standard deviation between the experimental curve and each polynomial; the polynomial of minimum deviation is adopted as the one best suiting that particular XSTATION. The average front position $\overline{Y}$ and the front standard deviation σ are then computed from the fitted curves. Various non-dimensional forms of $\overline{Y}$ and σ are finally given by combining with other wake characteristics as supplied by previous diagnostics of the axisymmetric wake. A similar procedure is followed with the table of numerical inputs (one set for each XSTATION) of zero frequency N versus radial position Y_N. The necessary curve-fitting polynomials are again at most of the 8th degree.

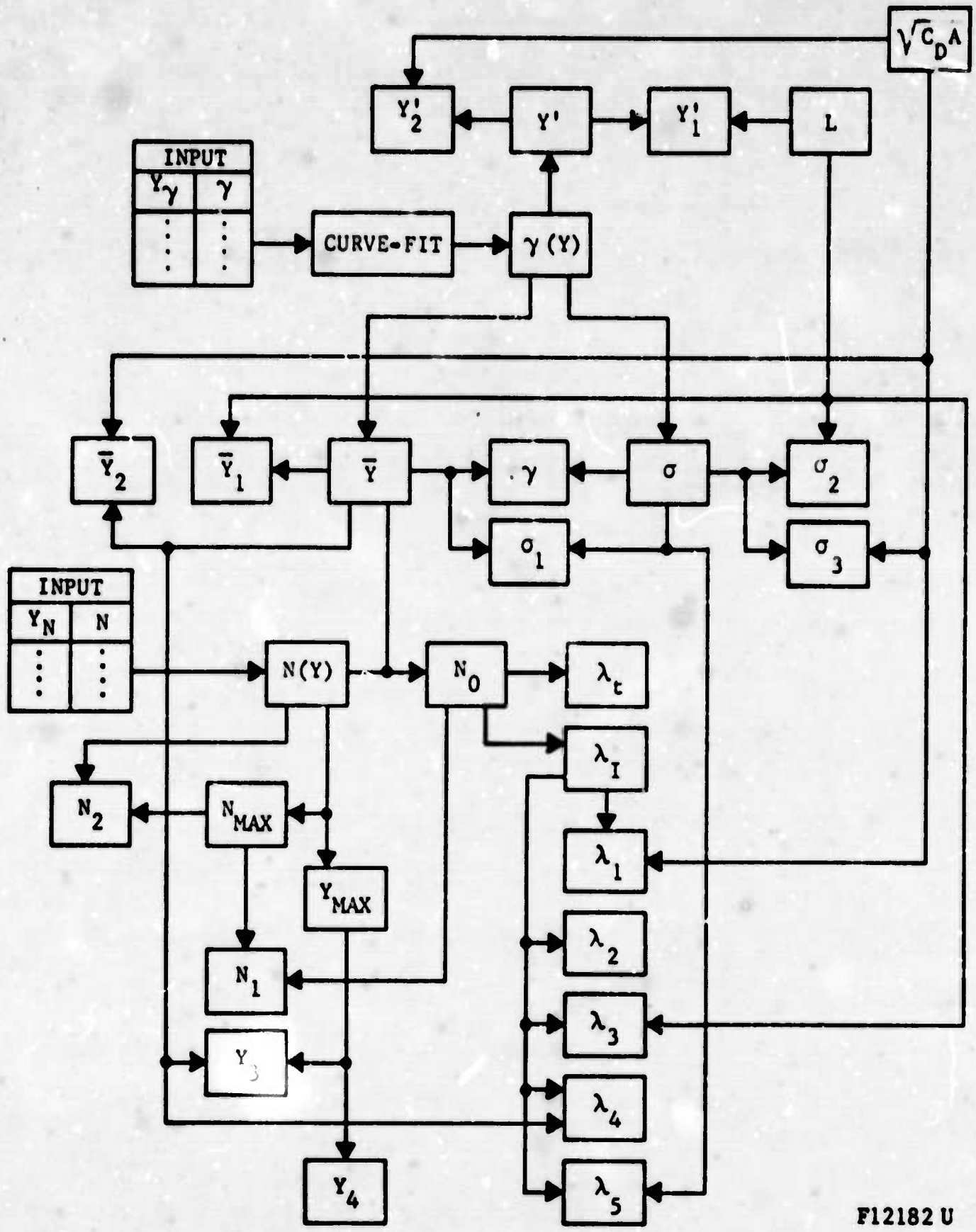

FIGURE A-1 WEB-VI PROGRAM

The output sheets for γ include the following: axial position $\bar{X}$ (XBAR), $\bar{Y}$ (YBAR), σ (SIGMA), $\sigma_1 = \sigma/\bar{Y}$ (SIGMA1), $\sigma_2 = \sigma/L$ (SIGMA2), $\sigma_3 = \sigma/\sqrt{C_D A}$ (SIGMA3) $\bar{Y}_1 = \bar{Y}/L$ (YBAR1), $\bar{Y}_2 = \bar{Y}/\sqrt{C_D A}$ (YBAR2) and Y', which is the maximum of the probability curve $d\gamma/dY$; also, $Y_1 = Y'/L$ (Y1PRIME) $Y_2' = Y'/\sqrt{C_D A}$ (Y2PRIME), and the fitted curve coefficients and standard deviation. In columnar form one obtains the following Y_γ (Y-GAMMA): γ (GAMMA), $(Y-\bar{Y})/\sigma$ (ZETA) and η (ETA).

The output sheets for N include the following at each $\bar{X}$: N_o (NO), $\lambda_t = \sqrt{2/\pi N_o}$ (LAMBDA-T), $\lambda_I = \lambda_t u_\infty$ (LAMBDA-I), $\lambda_1 = \lambda_I/\sqrt{C_D A}$ (LAMBDA-1), $\lambda_2 = \lambda_I/D$ where D is the cylinder model diameter (LAMBDA-2) $\lambda_3 = \lambda_I/L$ (LAMBDA-3), $\lambda_4 = \lambda_I/\bar{Y}$ (LAMBDA-4), $\lambda_5 = \lambda_I/\sigma$ (LAMBDA-5), N_{max} (N-MAX), $Y_{max} = Y_N(N_{max})$ (Y-MAX), $N_1 = N_{max}/N_o$ (N1), $Y_3 = Y_{max}/\bar{Y}$ (Y3) and also the coefficients of the fitted polynomial and its standard deviation. In columnar form at each $\bar{X}$ one obtains the following as a function of Y_N: N, $Y_4 = Y_N/Y_{max}$ (Y4), $N_2 = N/N_{max}$ (N_2) and η (ETA).

Typical results are shown on Figures A-2 and A-3.

WEB-VI PROGRAM WAKE BOUNDARY STRUCTURE A. DEMETRIADES
••DR55F USES WEB DATA ONLY FORMULATED MARCH 1967

X-STATION 2 XBAR 26.49514 YBAR 0.1271 SIGMA 0.0448 SIGMA1 0.3521 SIC

SIGMA3 0.5278 YBAR1 2.0565 YBAR2 1.4989 YPRIME 0.1210 Y1PRIME 1.95744 Y2

SIGMA CURVE FITTING CONSTANTS FOR POLY. OF DEGREE 7
A1= 0.99925578+000 A2= 0.12962074+001 A3= -0.13854382+003 A4= 0.41925195+004 A5= -0.64246750+005
A6= 0.44263025+006 A7= -0.13928845+007 A8= 0.16480960+007

RBAR 0.149113-002 SIGMA 0.106670-001

Y-GAMMA	GAMMA	ZETA	ETA
0.	1.0000	-2.8399	0.
0.0156	0.9950	-2.4914	0.2939
0.0312	0.9870	-2.1428	0.5339
0.0468	0.9650	-1.7943	0.7547
0.0624	0.9250	-1.4458	0.9793
0.0780	0.8620	-1.0973	1.2120
0.0936	0.7460	-0.7487	1.4534
0.1092	0.6600	-0.4002	1.7048
0.1248	0.4750	-0.0517	1.9643
0.1404	0.3250	0.2969	2.2281
0.1560	0.2200	0.6454	2.4942
0.1716	0.1500	0.9939	2.7605
0.1872	0.0900	1.3425	3.0264
0.2028	0.0450	1.6910	3.2917
0.2184	0.0200	2.0395	3.5562
0.2340	0.0060	2.3880	3.8194
0.2496	0.0010	2.7366	4.0816
0.2652	0.	3.0851	4.3428
0.2808	0.	3.4336	4.6030
0.2964	0.	3.7822	4.8623
0.3120	0.	4.1307	5.1209
0.3276	0.	4.4792	5.3790
0.3432	0.	4.8277	5.6367
0.3588	0.	5.1763	5.8938
0.3744	0.	5.5248	6.1503
0.3900	0.	5.8733	6.4066

A-2 FIGURE A-2. SAMPLE OUTPUT OF THE WEB-VI PROGRAM: INTERMITTENCY RESULTS

WEB-VI PROGRAM WAKE BOUNDARY STRUCTURE A. DEMETRIADES
••0455F USES WEB DATA ONLY FORMULATED MARCH 1967

X-STATION 6

NO 29313.239 LAMBDA-T 0.000015 LAMBDA-I 0.961091

LAMBDA-1 4.46175 LAMBDA-2 2.42700 LAMBDA-3 4.85400 LAMBDA-4 2.61796 LAMBDA-

N-MAX 30258.681 Y-MAX 0.16628 N1 1.0323 Y3= 1.150493

N CURVE FITTING CONSTANTS FOR POLY. OF DEGREE 6
B1= -0.21154089+003 B2= 0.53996853+C06 B3= -0.18371828+008 B4= 0.27336586+009
B5= -0.16862092+010 B6= 0.45113536+010 B7= -0.43789356+010

RBAR 0.412400+001 SIGMA 0.108760+004

YN	N	Y4	N2	ETA
0.	0.	0.	C.	0.
0.025	4500.	0.1503	C.1487	0.381
0.050	7000.	0.3007	0.2313	0.678
0.075	9500.	0.4510	C.3140	0.978
0.100	13800.	0.6014	C.4561	1.283
0.125	22500.	0.7517	C.7436	1.593
0.140	27500.	0.8419	0.9088	1.782
0.150	31500.	0.9021	1.0410	1.910
0.160	30500.	0.9622	1.0080	2.038
0.175	29000.	1.0524	C.9584	2.233
0.190	27000.	1.1426	0.8923	2.429
0.200	26000.	1.2028	C.8593	2.560
0.225	15200.	1.3531	C.5023	2.891
0.250	9000.	1.5034	0.2974	3.221
0.300	1000.	1.8041	0.0330	3.881
0.350	0.	2.1048	C.	4.538
0.400	0.	2.4055	C.	5.191
0.450	0.	2.7062	C.	5.962

FIGURE A-3. SAMPLE OUTPUT OF THE WEB-VI PROGRAM: ZERO-FREQUENCY RESULTS

APPENDIX B

BEHAVIOR OF A CLIPPED RANDOM VARIABLE

B.1. BASIC STATISTICS

Consider a stationary random function f (t) such as shown on Figure B.1. This "clipped" variable closely resembles the time history of the output of a sensor held fixed at some distance from the axis of turbulence, except that the tops of the jumps in f(t) are now considered flat. This waveform then resembles even closer the Schmidt trigger output of the intermittency circuit employed in this work. Define by f_1 and f_2 the values of f at the two extremes (related, say, to the sensor being outside and inside the turbulence respectively) separated by a constant H. Similarly Δt_1 and Δt_2 refer to time intervals outside and inside the turbulence, and intermittency γ over a long interval T is defined by

$$\gamma \equiv \frac{\overset{T}{\underset{0}{\Sigma}} \Delta t_1}{T}, \quad T = \Sigma\Delta t_1 + \Sigma\Delta t_2$$

and

$$\frac{\Sigma\Delta t_2}{T} = \frac{T - \Sigma\Delta t_1}{T} = 1 - \gamma$$

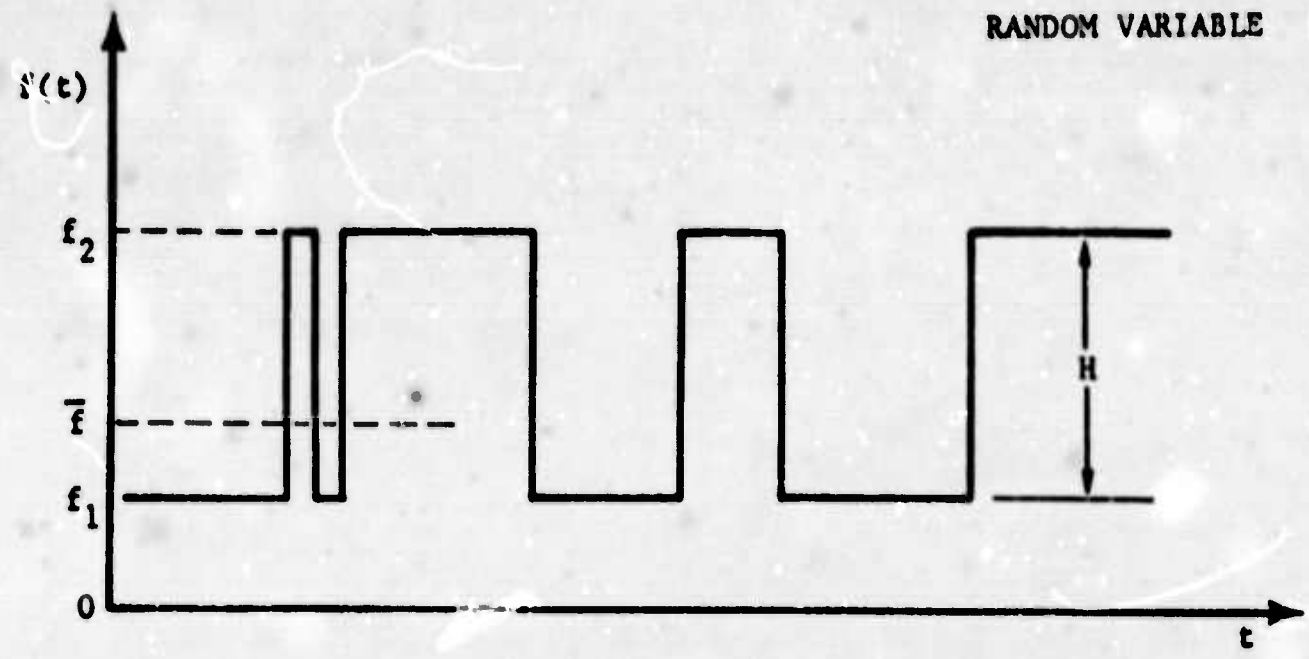

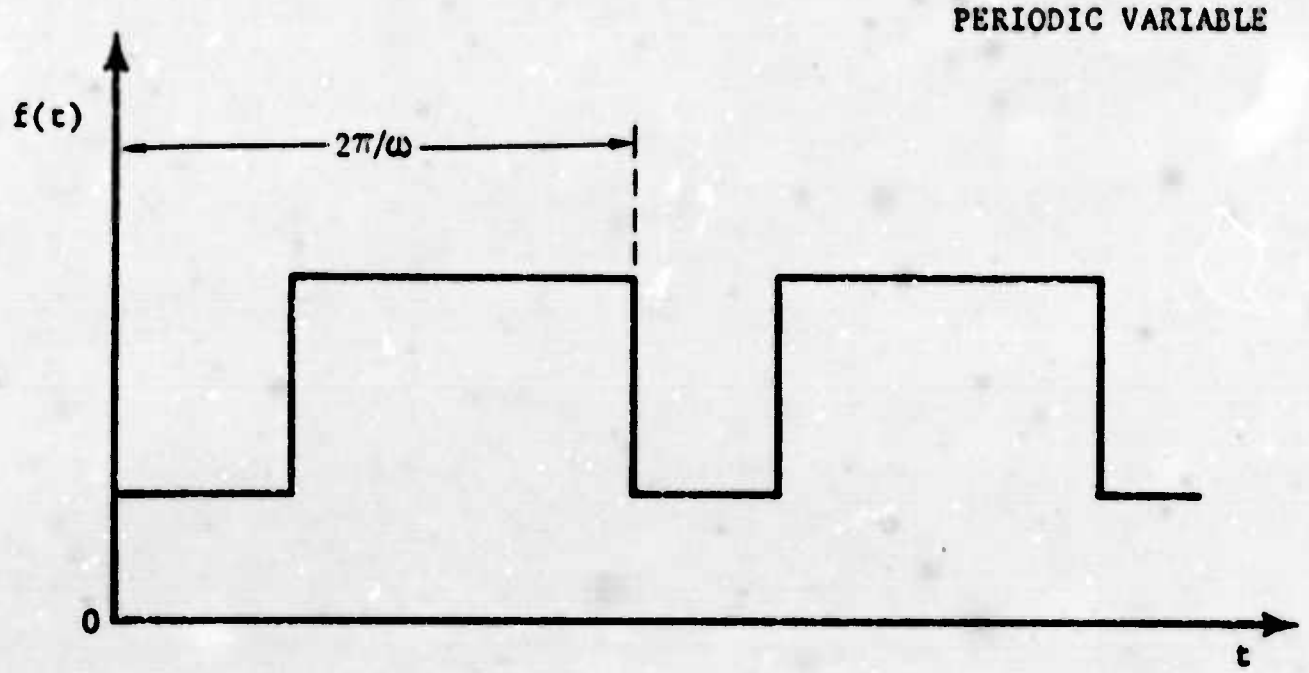

FIGURE B-1. TYPICAL TIME HISTORY OF A CLIPPED RANDOM VARIABLE

The mean value of f(t) now is

$$\bar{f} = \frac{1}{T}\int_0^T f\,dt = \frac{1}{T}\Sigma f_1 \Delta t_1 + \frac{1}{T}\Sigma f_2 \Delta t_2$$

$$= (1-\gamma) f_1 + \gamma(f_1+H) = f_1 + H\gamma \qquad \text{(B-1)}$$

which reduces to the obvious results

$$\bar{f}(\gamma=0) = f_1$$

$$\bar{f}(\gamma=1) = f_1 + H$$

The mean-square of the variance (fluctuation) of f(t) is

$$\overline{(\Delta f)^2} = \overline{[f-\bar{f}]^2} = \frac{1}{T}\int_0^T (f-\bar{f})^2 dt$$

with f equal to $f_1 + H$ or f_1 as appropriate and $\bar{f}$ given by (B-1). The result is

$$\overline{(\Delta f)^2} = \gamma H^2(1-\gamma) \qquad \text{(B-2)}$$

Here we distinguish two important limits. First, let

$$f_1 = 0$$

which gives

$$\frac{\overline{(\Delta f)^2}}{\bar{f}^2} = \frac{\gamma H^2(1-\gamma)}{H^2\gamma^2} = \frac{1}{\gamma} - 1$$

which is infinite at $\gamma = 0$. Physically, this is to be expected at the extreme edge of the turbulence zone for situations where the external (ambient) value of the observable f is zero. Such a case should theoretically occur, for example, when f is a contaminant density and the environment is completely devoid of this contaminant.

The other extreme occurs when $f_1 \gg H$. Then, $\bar{f} \simeq f_1$ and

$$\frac{\overline{(\Delta f)^2}}{\bar{f}^2} = \gamma(1-\gamma)\frac{H^2}{f_1} \ll 1$$

This value is representative, for example, in the present wake experiment where the jumps in all observables (velocity, temperature, etc.) are rather weak across the interface.

B.2. PERIODIC VARIABLE

Equations (B-1) and (B-2) are true regardless how the rectangular waves of f(t) are arranged. Consider, now, that the pattern repeats itself in time at regular intervals $2\pi/\omega$ of circular frequency ω; the intermittency factor γ retains its previous definition. We are interested in the spectrum of this periodic clipped function. The Fourier series describing the function is given (Reference 21) by

$$f(t) = \gamma H + \frac{2H}{\pi}\sum_{n=1}^{\infty}\frac{\sin n\pi\gamma}{n}\left[\cos n\omega t\cos\frac{n\pi\gamma}{2} - \sin n\omega t\sin\frac{n\pi\gamma}{2}\right]$$

$$= \gamma H + \sum_{1}^{\infty}(A_n \cos n\omega t + B_n \sin n\omega t)$$

where H is the constant height of the rectangular waves. The spectrum of f(t) can now be constructed since the mean square intensity of the Fourier components is given by

$$\frac{2H^2}{\pi^2}\frac{\sin^2 n\pi\gamma}{n^2} \equiv \text{mean-square of component } n$$

which, of course, becomes zero for $\gamma = 0,1$. In this spectrum the most intense component is the fundamental ($n = 1$) with gradually weakening higher harmonics at integral values of the fundamental frequency.